



Study for CO₂ separation with poly(ethylene oxide terephthalate)-poly (butylene terephthalate) multiblock copolymer membranes: Approaching a greener solvent preparation

Íñigo Martínez-Visus^{a,b}, Carlos Téllez^{a,b,*}, Joaquín Coronas^{a,b} 

^a Instituto de Nanociencia y Materiales de Aragón (INMA), CSIC-Universidad de Zaragoza, Zaragoza 50018, Spain

^b Chemical and Environmental Engineering Department, Universidad de Zaragoza, Zaragoza 50018, Spain

ARTICLE INFO

Keywords:

Gas separation
PolyActive™
Green solvent
Time lag
Transport properties

ABSTRACT

Green solvent alternatives for the multiblock copolymer PolyActive™ were selected to test their effectiveness in membrane fabrication for gas separation. Solubility tests were conducted to assess the solvent-polymer compatibility, followed by membrane fabrication using a drop casting-solution method. Ethyl lactate was identified as a potential greener solvent, compared to more commonly used solvents like chloroform and tetrahydrofuran, as it maintained the membrane conformation, thermal and chemical stability, and thermal degradation characteristics as demonstrated by membrane characterization using SEM, FTIR, TGA and DSC. Single gas transport parameters (permeability, diffusivity and solubility) for N₂, H₂, CH₄, He and CO₂ were obtained via the time-lag method for the prepared membranes. A temperature dependence study was conducted in the 25–70 °C range, calculating activation energies for gas transport properties and ideal selectivities. Mixed gas measurements were also performed, comparing separation selectivities to those (ideal selectivities) obtained in single gas, indicating a potential competitive adsorption effect between less permeable species, leading to more selective separation in gas mixture. Membranes prepared with different polymer concentrations (1, 2 and 5 wt%) in ethyl lactate achieve a CO₂/N₂ ideal selectivity of up to 50.4 at a CO₂ permeability of 179 Barrer. This enhanced performance was attributed to ethyl lactate higher boiling point, resulting in a more densely packed polymer structure as reflected by the higher crystallinity and lower fractional free volume measured through XRD, DSC and pycnometry analyses.

1. Introduction

Emission of greenhouse gases, mainly from fossil fuel-based energy production processes, has become the leading cause for global warming, significantly impacting climate change through their accumulation in the atmosphere [1]. Carbon dioxide (CO₂), the most prevalent greenhouse gas and the primary contributor to global warming, has steadily increased its concentration in the atmosphere over the last decades, from 340 to 423 ppm. It is projected to rise and stabilize to at least the 450 ppm level in the next 30 years, under the most optimistic scenarios [2]. Carbon capture, utilization and storage (CCUS) technologies are used to prevent CO₂ emissions from their source, such as in exhaust gases from post-combustion processes, combustible gas streams in pre-combustion or oxy fuel-combustion. These technologies involve multiple steps, like subsequent purification, transportation and either

utilization (e.g., as a reactant for chemical or fuel production) or storage/sequestration [3]. Common CO₂ capture methods from flue gas include adsorption, absorption and cryogenic distillation. However, these approaches have drawbacks: regeneration of sorbents/solvents, potential toxicity or intensive energy consumption [4].

Membrane separation has emerged as an attractive alternative method in the recent years, receiving significant attention and investment due to its economic viability, scalability, environmental friendliness, and lower energy requirements [5,6]. Research on membrane technologies for CCUS focuses on the developing of highly selective materials to CO₂ that possess good mechanical and chemical stability, as well as an easy processability into membrane conformation [7]. Multi-block copolymer membranes offer desirable properties by combining two alternating polymer segments: flexible (soft) highly gas-permeable segments, such as such as polyethylene oxide (PEO),

* Corresponding author at: Instituto de Nanociencia y Materiales de Aragón (INMA), CSIC-Universidad de Zaragoza, Zaragoza 50018, Spain.

E-mail address: ctellez@unizar.es (C. Téllez).

<https://doi.org/10.1016/j.jece.2025.116893>

Received 16 December 2024; Received in revised form 21 April 2025; Accepted 30 April 2025

Available online 4 May 2025

2213-3437/© 2025 The Author(s). Published by Elsevier Ltd. This is an open access article under the CC BY-NC-ND license (<http://creativecommons.org/licenses/by-nc-nd/4.0/>).

which also have a high CO₂ affinity, with rigid (hard) segments that provide mechanical and thermal stability [8]. Among these materials, poly(ethylene oxide terephthalate)-poly(butylene terephthalate) (PEOT-PBT) block copolymers, marketed as PolyActive™, have shown promising in CO₂/N₂ separation. By tailoring the molecular weight of PEO (1500 Da) and the soft/hard block ratio (77/23), referred here as PolyActive™ 1500, high separation selectivity — reaching up to 50 — and significant permeability have been achieved, outperforming other well-known poly(ether-amides) like Pebax® [9,10]. PolyActive™ 1500 has also demonstrated its applicability in pilot plant for flue gas and biogas separation [11]. In recent years, it has gained greater attention as more advanced and extensive research focuses on its potential for industrial applications. Numerical and experimental studies on the roll-to-roll coating process for thin-film composite (TFC) PolyActive™ membranes have also emerged. This method, which is well-established, supports scalability and enhances the commercial feasibility of PolyActive™ membranes [12]. Moreover, more comprehensive energy cost studies involving real flue gas streams, including impurities such as SO₂, NO_x, particulates, H₂S and the effects of humidity on separation performance, are being conducted using PolyActive™ as the membrane material [13,14]. Since it was introduced more than a hundred years ago [15], the time-lag method has been widely used to characterize the gas separation properties of different polymeric membranes [16–19]. Most polymers have been studied in depth using this methodology, although it has certain limitations since individual gases are measured, which may be different when gas mixtures are involved [20]. In this sense, for PolyActive™ 1500, an in-depth time-lag study and comparison with binary mixtures is still needed.

One of the main concerns for industrial application is the sustainability and environmental impact in new processes, particularly in terms of energy and economic savings due to waste treatment and pollutant reduction. Membrane fabrication often involves the use of large amounts of non-degradable, flammable, highly-volatile, toxic and non-renewable solvents [21]. In case of PolyActive™, although different formulations can be used, the solvents reported in the literature are predominantly limited to chloroform (CHCl₃) [9,22,23], tetrahydrofuran (THF) [24–27] and occasional mixtures with CHCl₃-dioxane [28], all of which are hazardous with significant safety, health and environmental risks. There is a strong interest in identifying green solvents compatible with PolyActive™ that could serve as alternatives to these traditional solvents. Ideally, these solvents not only should make the membrane preparation process greener but also align with the “Twelve Principles of Green Chemistry”, minimizing waste, using renewable and sustainable sources, maximizing material efficiency, reducing energy consumption and toxicity and incorporating catalytic reagents, among others [29]. To this end, a range of greener solvents (acetone, ethyl acetate, 1-propanol, 1-butanol, ethyl lactate and 1-octanol) were selected, along with conventional solvents (CHCl₃ and THF), for solubility tests to identify potential alternatives for fabricating PolyActive™ 1500 membranes.

Moreover, hollow fiber (HF) membranes remain particularly attractive for industrial applications due to their high surface area-to-volume ratio, enabling compact, efficient separation modules. However, transitioning toward greener manufacturing methods introduces notable challenges [30]. One key issue lies in identifying sustainable solvents that can facilitate the fabrication of HF without compromising the membrane performance or scalability. Many green solvents exhibit high viscosities and boiling points, which, while advantageous for safety and environmental reasons, complicate the spinning and coating processes. These properties can lead to irregular fiber formation, non-uniform coating layers and slower phase inversion kinetics, demanding careful tuning of fabrication parameters. Recent advances in green solvents, such as thymol [31], ethyl lactate [32], and plant-based p-cymene [33], have shown promise in the fabrication of thin-film composite (TFC) membranes, enabling stable dope solutions, continuous hollow fiber spinning and improved membrane performance, including hydrophilicity, antifouling and superhydrophobicity for

efficient separations. These innovations highlight the growing potential of green solvents to enable sustainable, high-performance HF and TFC membranes without relying on traditional toxic solvents.

In this study, PolyActive™ 1500 was dissolved in selected greener solvents, and their compatibility with the membrane fabrication process using the casting-solution method was investigated. Ethyl lactate was identified as a promising alternative green solvent, and the effect of polymer concentration in the casting solution on membrane performance was evaluated. The resulting membranes were physicochemically characterized. Gas permeation tests were conducted to determine key gas separation parameters, including permeability, ideal selectivity, diffusion and solubility for various gases (N₂, H₂, CH₄, He and CO₂), using single gas measurements via the time-lag technique. These results were compared to those achieved with membranes prepared with traditional solvents to assess the potential of this proposed green solvent. Additionally, to further explore the separation performance, CO₂/N₂ and CO₂/CH₄ gas mixtures were tested, simulating CO₂ capture in post-combustion and methane upgrading processes, respectively. Both single-gas and mixed-gas separation performances were analyzed and compared. To our knowledge, although ethyl lactate has been studied for membrane fabrication with other polymers, such as PLA [34,35], this is the first study where it has been successfully used for gas separation membrane fabrication with a multiblock copolymer like PolyActive™ 1500.

2. Materials and methods

2.1. Materials

PEOT-PBT multi-block copolymer, commercially known as PolyActive™, was purchased in the form of pellets from PolyVation, Netherlands. The designated composition of the copolymer had a relative weight percentage of soft (PEOT) to hard segment (PBT) of 77:23, and a molecular weight for the polyethylene oxide chain (PEO) in the soft segment of 1500 g·mol⁻¹ (from now on referred as PolyActive™ 1500).

Solvents, chloroform (CHCl₃, >99 %) tetrahydrofuran (THF, >99.95 %), ethyl lactate (98 %), 1-propanol (99.5 %) were purchased from Sigma Aldrich, Germany, 1-octanol (99 %), 1-butanol (99.8 %) were purchased from Scharlab S.L., Spain, acetone (99 %) was provided by Productos Gilca SC., Spain, and Ethyl Acetate were purchased from Thermo Fisher, Spain.

Gases used for permeation tests were research-grade: hydrogen, helium, nitrogen, argon (each >99.999 % pure), carbon dioxide (>99.995 %) and methane (>99.95 %) and supplied by Linde Gas España S.A.U., Spain.

2.2. Membrane preparation

PolyActive™ 1500 membranes were prepared following the casting-solution method with different solvents (Table 1). The selection of these solvents aimed to identify greener alternatives to the commonly used PEOT-PBT solvents, chloroform and tetrahydrofuran [25,28,36,37]. In general, polymer pellets (0.35 g) were firstly dried in an oven at 100 °C for 1 h and cooled down before introducing them in a round bottom flask with the desired solvent (2 wt%). Solutions were put under reflux at a certain temperature and time until pellets were completely dissolved or for a maximum of 8 h (Table 2). The casting solutions were cooled down to room temperature, and if no reprecipitation of the polymer occurred they were poured onto Petri dishes covered with perforated aluminum foil and left evaporate for at least 3 days. Finally, obtained membranes with a thickness of 70–90 μm were heated at 80 °C under vacuum for at least 6 h to remove remains of solvent and peeled off from the Petri dish storing them for later gas permeation tests.

Table 1

Solvents selected for solubility study. Structural formula, boiling point (T_B) and molar volume of the solvents used in solubility tests for PolyActive™ 1500.

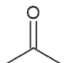
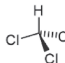

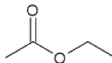
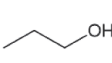
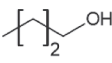
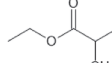
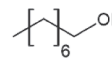
Solvent	Acetone	Chloroform	Tetrahydrofuran	Ethyl Acetate	1-Propanol	1-Butanol	Ethyl Lactate	1-Octanol
Formula								
T_B (°C)	56	61.2	66	77.1	97	117.7	154	195.0
Molar volume (cm ³ ·mol ⁻¹)	73.8	80.5	81.9	98.6	75.1	92	115	157.7

Table 2

Reflux conditions used for dissolution of PolyActive™ 1500 pellets. Temperature and time required for the solvents tested, observed solubility of the polymer and calculated distance in Hansen space (R_a).

Solvent	Polymer Conc. (wt%)	Reflux Conditions		Solubility	R_a (MPa ^{0.5})
		T (°C)	Time (h)		
Acetone	2	60	8	Insoluble	6.2
Chloroform	2	RT	2	Soluble	3.5
Tetrahydrofuran	2	70	4	Soluble	2.3
Ethyl acetate	2	80	8	Partially soluble	4.1
1-Propanol:1-butanol (3:1)	2	110	8	Partially soluble ^a	10.6
Ethyl lactate	1, 2, 5	80	4	Soluble	6.7
1-Octanol	2	120	8	Partially soluble ^a	6.0

^a Precipitation of polymer (clouded solution) occurred during cooling.

2.3. Membrane characterization

2.3.1. Membrane characterization

Scanning electron microscopy (SEM) images of the cross-section of the membranes were obtained with an Inspect F50 model scanning electron microscope (FEI, operated at 10 kV). Samples were prepared by fracturing the membranes under liquid N₂, fixed in a sample holder with conductive carbon tape and coated with palladium. Thermogravimetry analysis (TGA) for thermal stability determination was performed with a Mettler Toledo TGA/STDA 851e where small pieces of membrane or pellet (2–4 mg) were placed in 70 mL alumina pans and heated under nitrogen air flow (50 cm³(STP)·min⁻¹) from 35 to 700 °C at a heating rate of 10 °C·min⁻¹. Differential scanning calorimetry (DSC) analyses were performed using a DSC Q20 with a refrigerated cooling system (RCS90). Samples (3–5 mg) were placed in a hermetic aluminum pan and firstly heated to 100 °C and cooled down to –50 °C (10 °C·min⁻¹), afterwards the samples were put under two heating-cooling cycles from –50–200 °C with a heating ramp of 10 and 20 °C·min⁻¹, respectively. X-ray diffraction (XRD) measurements of the prepared membranes were performed using a reflection-transmission spinner stage with a zero-background sample holder on a PANalytical Empyrean-Multipurpose (Cu K α). Fourier transform infrared spectroscopy (FTIR) was conducted with a Bruker Vertex 70 FT-IR provisioned with a DTGS detector and a Golden Gate diamond attenuated total reflectance (ATR) accessory. The spectra were recorded by averaging 40 scans in the 4000–600 cm⁻¹ wavenumber range at a resolution of 4 cm⁻¹. Viscosity tests were conducted with a SMART L Fungilab Rotational viscometer, where polymer casting solutions were poured in a APM/B adapter (6.7 mL) and a TL5 spindle was used for to subject the samples to different rotational speeds

(from 20 to 200 rpm) at 20 °C. Dynamic light scattering (DLS) spectroscopy was conducted on a Brookhaven 90 Plus instrument to measure the hydrodynamic size of the dissolved polymer in the different solvents applied. For valid measurements, the sample count rate exceeded 50 kcps. Glass vials were filled with casting solutions containing 4 wt% PolyActive™ 1500, whose solvent was filtered through a 0.22 micron PTFE filter before use. Also, the viscosity values obtained in rotational viscometer measurements were used for size distribution calculation from DLS correlation curves. Membrane surface roughness was analyzed using atomic force microscopy (AFM) using a Bruker Multimode 5 AFM System equipped with a J-type scanner (200 μ m(X) x 200 μ m(Y) x 5 μ m(Z), RTESPA-150, 5 N·m⁻¹ symmetric tip, aluminum reflex coating). Measurements were performed on three different areas of each membrane, with an image size of 5 \times 5 μ m². Static water contact angle (WCA) measurements of the membranes were performed at room temperature using a Krüss Drop Shade Analyzer 10 MK2. Measurements were taken at a minimum of four different areas on each membrane, using a droplet volume of 4 μ L. Also, intrinsic WCA was estimated following Wenzel equation and roughness from AFM measurements. The fractional free volume (FFV) of the prepared membranes was estimated from the specific skeletal volume (V_0) obtained via helium pycnometry (Micromeritics AccuPyc 1330) [38], and the specific apparent volume (V) was determined using a 25 mL pycnometer for solids with water as the auxiliary liquid [39]. Before measurements, the membranes were dried in a vacuum oven at 70 °C for 4 h and then temperature-stabilized at room temperature. The equation used for the FFV calculations is:

$$FFV(\%) = \frac{V - V_0}{V} \cdot 100 \quad (1)$$

2.3.2. Gas transport properties

The gas transport properties (permeability, apparent diffusivity and solubility) of pure nitrogen, hydrogen, methane, helium and carbon dioxide were measured by the constant volume/pressure increase time-lag method [40]. Pressure in the permeate side of the membrane increases gradually until reaching a steady state, where the slope becomes constant. The permeability coefficient P (Barrer, 10⁻¹⁰ cm³(STP)·cm·cm⁻²·s⁻¹·cmHg⁻¹) of a pure gas (i) was calculated as:

$$P_i = \frac{V_d \cdot l \cdot T_0}{A \cdot T \cdot p_{u,0} \cdot p_0} \cdot \frac{dp_d}{dt} \quad (2)$$

where V_d is the constant permeate volume in cm³ (STP), l is the membrane thickness in cm, T_0 is 273.15 K, A is the effective membrane area in cm², T is the experiment temperature in K, $p_{u,0}$ is the feed pressure in cmHg, p_0 is 76 cmHg and dp_d/dt is the slope of the permeate pressure curve in the steady state region in cmHg·s⁻¹.

The apparent diffusion coefficient D_i (cm²·s⁻¹) was calculated from the membrane thickness (l in cm) and time-lag (θ_i in s), estimated graphically as intersection of the tangent of the steady state pressure

curve with the horizontal time axis:

$$D_i = \frac{l^2}{6 \cdot \theta_i} \quad (3)$$

For dense membranes, where typically transport of the species follows the solution-diffusion mechanism, the apparent solubility coefficient ($\text{cm}^3(\text{STP}) \cdot \text{cm}^{-3} \cdot \text{cmHg}^{-1}$) was calculated as the ratio between permeability and diffusivity as follows:

$$S_i = \frac{P_i}{D_i} \quad (4)$$

Gas transport parameters in polymers, such as permeability and diffusion, are highly temperature-dependent, as they are activated processes that follow an Arrhenius exponential law. Consequently, the activation energies for permeability (E_p) and diffusion (E_D) can be estimated using Eqs. 5 and 6 [41]. Since solubility can be derived from gas transport parameters according to Eq. 4, the apparent heat of adsorption (ΔH_S) can also be estimated [42]:

$$P_i = P_{0,i} \cdot e^{-\frac{E_{p,i}}{RT}} \quad (5)$$

$$D_i = D_{0,i} \cdot e^{-\frac{E_{D,i}}{RT}} \quad (6)$$

$$S_i = S_{0,i} \cdot e^{-\frac{\Delta H_{S,i}}{RT}} \quad (7)$$

where P_0 , D_0 and S_0 are the pre-exponential factors (Barrer, $\text{cm}^2 \cdot \text{s}^{-1}$ and $\text{cm}^3(\text{STP}) \cdot \text{cm}^{-3} \cdot \text{cmHg}^{-1}$ respectively), R is the ideal gas constant ($8.314 \text{ J} \cdot \text{mol}^{-1} \cdot \text{K}^{-1}$) and T is the temperature in K.

Ideal selectivity is calculated as the ratio of individual permeabilities of the two species:

$$\alpha_{i/j} = \frac{P_i}{P_j} \quad (8)$$

For binary gases, permeability of each of the species (P_i in Barrer) was also calculated in mixed gas separation tests using the following equation:

$$P_i = \frac{Q_i \cdot l}{\Delta p_i \cdot A} \quad (9)$$

where Q is the permeate flow through the membrane in $\text{cm}^3(\text{STP}) \cdot \text{s}^{-1}$ and Δp_i denotes the partial pressure difference of gas i between the feed and permeate sides in cmHg. Using pressures instead of fugacities was justified since the absolute pressures in the measuring system were sufficiently low [10].

The efficiency of separating mixed gases in a binary mixture can be reflected with the separation selectivity using the Eq. 8 calculated with permeabilities in the mixture or with the separation factor (SF), which is determined as the ratio of the concentrations of the two components (i and j) in feed (x) and permeate side (y) of the membrane module as follows:

$$SF_{i/j} = \frac{y_i/y_j}{x_i/x_j} \quad (10)$$

The separation factor is dependent on the separation selectivity, the pressure ratio between the feed and permeate sides, and the molar fraction of the permeable component in the feed. In cases of sufficiently high pressure ratios or diluted permeate concentrations, the SF approaches separation selectivity [43].

2.4. Gas permeation

2.4.1. Single gas separation tests

Time-lag experiments were conducted at various temperatures using a constant volume/pressure experimental setup (Fig. 1A). In these time-

lag method dense membranes were cut into circles with an area of 8.0 cm^2 and placed in a stainless steel module, which was then put inside of an oven (Mettmert UN55) to control the temperature for experiments at 25, 35, 50 and 70°C . Before each experiment, the system was evacuated with a vacuum pump (10^{-2} mbar) on both sides to remove any gas traces from the membrane and the upstream/downstream volumes. The upstream compartment was then filled with pure gas and stabilized at 3 bar prior to starting the experiment. During the experiment, the pressure on the permeate side was recorded with a pressure transducer and logged to a computer. To meet the boundary conditions of the time-lag method and achieve an effective steady-state of flux, the downstream pressure was kept much lower than the upstream pressure, with a maximum downstream pressure set at 0.1 % of the upstream pressure [42,44]. Subsequently, the single gas permeability for each testing gas (P_i) was calculated using the slope of the pressure curve in the steady-state region and Eq. 2, while the effective diffusion coefficient (D_i) was determined using Eq. 3. The effective solubility coefficient (S_i) was then calculated using P_i and D_i with Eq. 4. An order for measuring the gases was chosen based on their permeability, starting from the highest to the lowest, but always measuring CO_2 last. This approach minimizes the risk of inducing a plasticization into the membrane and affecting the measurements of other gases. Additionally, each gas is measured multiple times (usually four) until the gas separation properties, derived from analyzing their time-lag pressure curves, become stable.

2.4.2. Mixed gas separation tests

Membranes were cut into circles with an area of 12.6 cm^2 and secured in a stainless steel module, similar to the single gas measurements. To ensure no leakage, the module comprises two pieces which grip the membrane between a Viton O-ring and a macro-porous disk support (316 L Mott Co.). For gas separation measurements at 35°C , the permeation module was placed inside an oven (UNE 200 Mettmert). Binary gas mixtures were fed through Alicat Scientific mass flow controllers (MC-100CCM-D for CO_2 and MC-200CCM-D for the remaining gases), enabling a precise control of the different concentration ratios, with an accuracy of flowrate setpoint of less than $\pm 0.65\%$. The total gas flow for mixed gas mixtures was fixed at $100 \text{ cm}^3(\text{STP}) \cdot \text{min}^{-1}$, with molar compositions of CO_2/N_2 (15/85), CO_2/CH_4 (50/50) and CO_2/H_2 (50/50). The feed side pressure was maintained at 3 bar by regulating a needle valve at the retentate of the permeation module. The permeate side of the membrane was swept with $15 \text{ cm}^3(\text{STP}) \cdot \text{min}^{-1}$ of helium (argon in the case of measuring a mixture containing H_2) and operated at around atmospheric pressure ($\sim 1.1 \text{ bar}$). Concentrations of species in permeate side were analyzed online by an Agilent 990 micro-gas chromatograph. Measurements for the membranes were performed for at least 2 h, until steady-state of the permeate was reached. For all mixed gas experiments total stage cut (ratio between permeate and feed flow rate) was less than 0.5 %. Permeabilities for the gases fed were calculated in Barrer (Eq. 9), separation factors (SF) were obtained from the ratio of concentration in the feed and permeate side (Eq. 10) and separation selectivities were achieved as the ratio of the corresponding permeabilities (Eq. 8). A scheme of the mixed gas separation set up is shown in Fig. 1B.

3. Results

3.1. Solvent tests

Reflux conditions (temperature and time) in the polymer dissolution for the selected solvents are shown in Table 2. Casting solutions of chloroform and THF were completely clear without any trace of undissolved polymer pellets, in accordance with their widely use in literature for fabrication of PEOT-PBT membranes [26,45]. Tests with other solvents showed different results: solutions based on 1-octanol and propanol:butanol became cloudy after letting them cool down to room

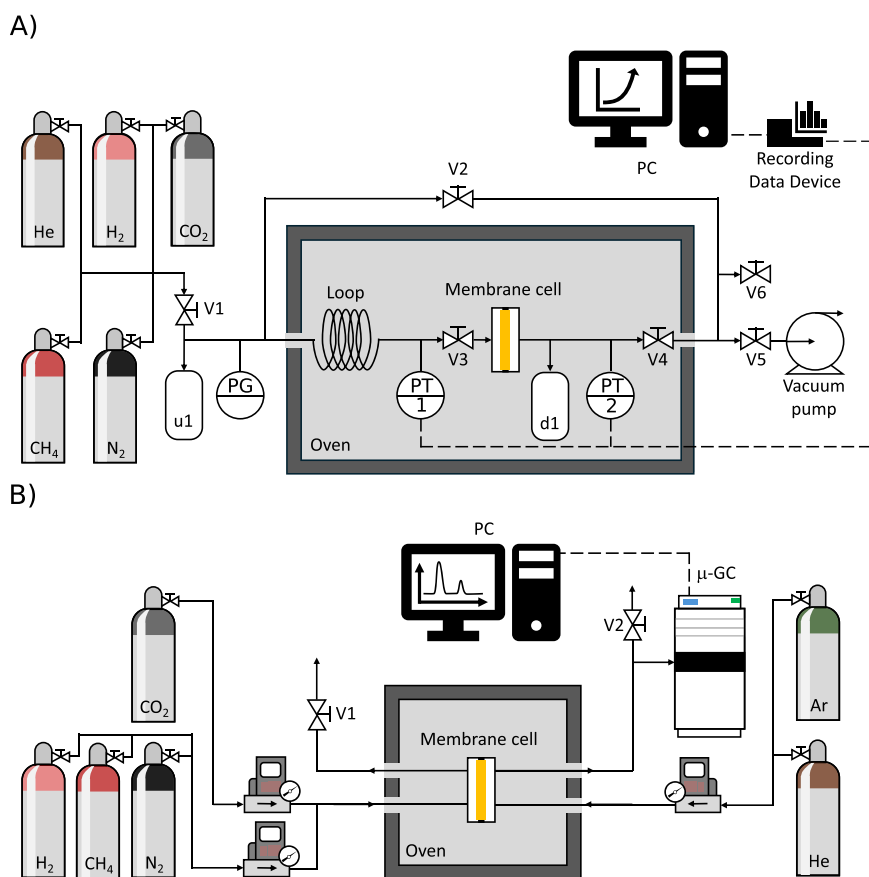


Fig. 1. Gas separation experimental set-ups for measurement of gas transport properties. Schematic diagram of the single gas measurement setup for time-lag method (A) and mixed gas separation setup used for membrane measurements (B). The mixed gases were supplied using laminar DP (differential pressure) mass-flow controllers, specifically CO₂ (Alicat Scientific, MC-100CCM-D) and H₂, CH₄, N₂, He and Ar (Alicat Scientific, MC-200CCM-D).

temperature. Ethyl acetate, despite being under reflux for 8 h, did not dissolve all pellets, even though the solution appeared clear. Similarly, acetone failed to dissolve the pellets under boiling point conditions after 8 h under reflux. However, ethyl lactate was found to be effective (requiring reflux for at least 4 h), as it dissolved all pellets and the casting solution remained clear after cooling to room temperature like when THF or chloroform was used as solvent.

Therefore, for this study ethyl lactate was selected as the potential new greener solvent due to its advantageous properties. It is derived from renewable sources, is biodegradable, non-toxic and easy to purify [46]. Casting solutions with varying polymer concentrations (1 and 5 wt %) were prepared to examine its impact on physical properties and gas separation performance. The 5 wt% solution exhibited an increased viscosity at room temperature, complicating the casting process. To better control the casting process and facilitate the evaporation rate, given that ethyl lactate is a high boiling point solvent (154 °C, see Table 1), the casting solutions were cooled to 60 °C (instead of room temperature), and the evaporation process for membrane formation was carried out in an oven maintained at 40 °C. Additionally, the time required for solvent evaporation was longer compared to those needed with CHCl₃ and THF with boiling points of 61.2 and 66 °C, respectively (see Table 1). Solutions containing higher polymer concentration (5 wt %) and less amount of solvent took 24 h to evaporate, while those with a lower polymer concentration (1 wt%) and more solvent required up to 4 days to completely evaporate.

The Hansen Solubility Parameters (δ_d , δ_p and δ_h) for PolyActive™ 1500 were estimated using HSPiP software based on the observed

solubility tests with the selected solvents (typically used in the casting of polymeric membranes), yielding values of 17.8, 6.3 and 7.0 in MPa^{0.5}, respectively.¹ The distance in Hansen space (R_a) was also calculated and is presented in Table 2. Smaller (R_a) values indicate stronger interactions (i.e. better compatibility) between the polymer and the solvent. Furthermore, based on these calculations, other potential solvents for PolyActive at room temperature could include cyclohexanone (R_a = 2.8 MPa^{0.5}), 1,3-dioxolane (2.4 MPa^{0.5}) and anisole (2.2 MPa^{0.5}).

However, these solvents were not studied here due to their lower greenness compared to ethyl lactate, as indicated by the SHE (Safety, Health and Environment) ranking from the American Chemical Society's solvent selection tool [47]. Furthermore, this solvent is biobased, which enhances its sustainable nature. Finally, the relatively unfavorable R_a value of ethyl lactate (6.7 MPa^{0.5} as compared, for instance, to 2.3 MPa^{0.5} and 3.5 MPa^{0.5} of THF and chloroform, respectively) was compensated by its greener character and the casting at 60 °C. Interestingly, the opposite behavior has been reported by Alqaheem et al. [48] for a similar solvent, methyl lactate, in the fabrication of a polyetherimide membrane. HSP predicted a lower R_a but polyetherimide was insoluble in a range of temperatures from 60 to 140 °C, while solvents with higher R_a could dissolve the polymer. This unexpected result was attributed to the HSP model not taking polymer morphology and solvent molecular size into account.

Solvents exhibiting partial solubility for the polymer could still be utilized for membrane fabrication, even if polymer precipitation occurs during the cooling of the casting solution. Using lower polymer concentrations or employing a heated Petri dish (hot-casting) would

¹ S. Abbott (personal communication, July 15, 2024).

facilitate the formation of polymeric membranes.

3.2. Membrane characterization

Dense PolyActive™ 1500 membranes were fabricated using casting-solution method with solvents that effectively dissolved the pellets: chloroform (2 wt%), tetrahydrofuran (2 wt%) and ethyl lactate (1,2 and 5 wt%) as detailed in Table 2. As previously mentioned, permeation through dense membranes operates via a solution-diffusion mechanism, allowing selective separation of gas species based on their differing solubility and diffusivity within the polymer matrix [49]. Cross-sectional SEM images in Figure S1 confirmed the non-porous nature of the prepared membranes. Furthermore, electron imaging revealed no significant differences in the conformation and average thickness of the membranes.

To assess the potential chemical changes caused by the solvents used in the casting process and their impact on the separation performance, the membranes were compared with pristine polymer pellets. Thermal stability was evaluated with TGA, Differential thermogravimetric analysis (DTG) and DSC analyses, as shown in Figs. S2a, S2b and 2a, respectively. TGA and DTG results indicated that both the pristine pellets and the prepared membranes behaved almost identical, with a single sharp mass loss at ca. 400 °C corresponding to polymer degradation, suggesting that the thermal degradation of both the soft and hard blocks of the polymer were apparently similar [50]. Additionally, all membranes showed a minor weight loss of less than 1 wt% up to 200 °C, likely due to absorbed water or residual solvents in the polymer.

The DSC thermograms (Fig. 2a) for the pristine pellets show two

melting endotherms. The first strong melting peak occurred around room temperature, from an onset temperature of 11.9 °C to an endset of 25.5 °C, corresponding to the PEOT soft block. The second melting peak, which was barely noticeable and very broad, appears at around 144 °C, corresponding to the PBT hard block [51]. As reported in literature [52], melting peaks for PBT blocks may not be detected if they are present in a low weight fraction (around 24 wt%) because sparse and short butylene terephthalate units cannot aggregate and crystallize effectively in large enough regions. During cooling, both phases showed exothermic crystallization peaks at lower temperatures than during heating. The PBT peak was at 94.4 °C, and the onset temperature for the PEOT crystallization peak was at 5.4 °C. Compared to the dense membrane thermograms, a slightly shift to higher temperatures for melting or crystallization onset, peak and inset temperatures were observed (Table S1). Showing a difference in polymeric chains thermal mobility after the commercial pellet fabrication versus the polymeric membranes by the solution-casting method. It is important to note that the PEOT soft blocks, whose main role is their CO₂-philicity, would melt at room temperature. As reported by Rahman et al. [53], when PolyActive™ membranes were tested at a temperature under the melting transition of the polyethylene glycol block, a noticeable shift in the gas separation performance behavior of the polymer occurred, primarily a drop in CO₂/N₂ selectivity and overall CO₂ permeability. For this reason, the minimum permeation temperature selected for this study (see below) was set at 25 °C, as the highest onset temperature measured for the crystallization of the soft block was 13.3 °C, where the PEOT block is in its melted state and the PBT block in a semicrystalline state. Additionally, by integrating the PEOT block melting peak an approximated

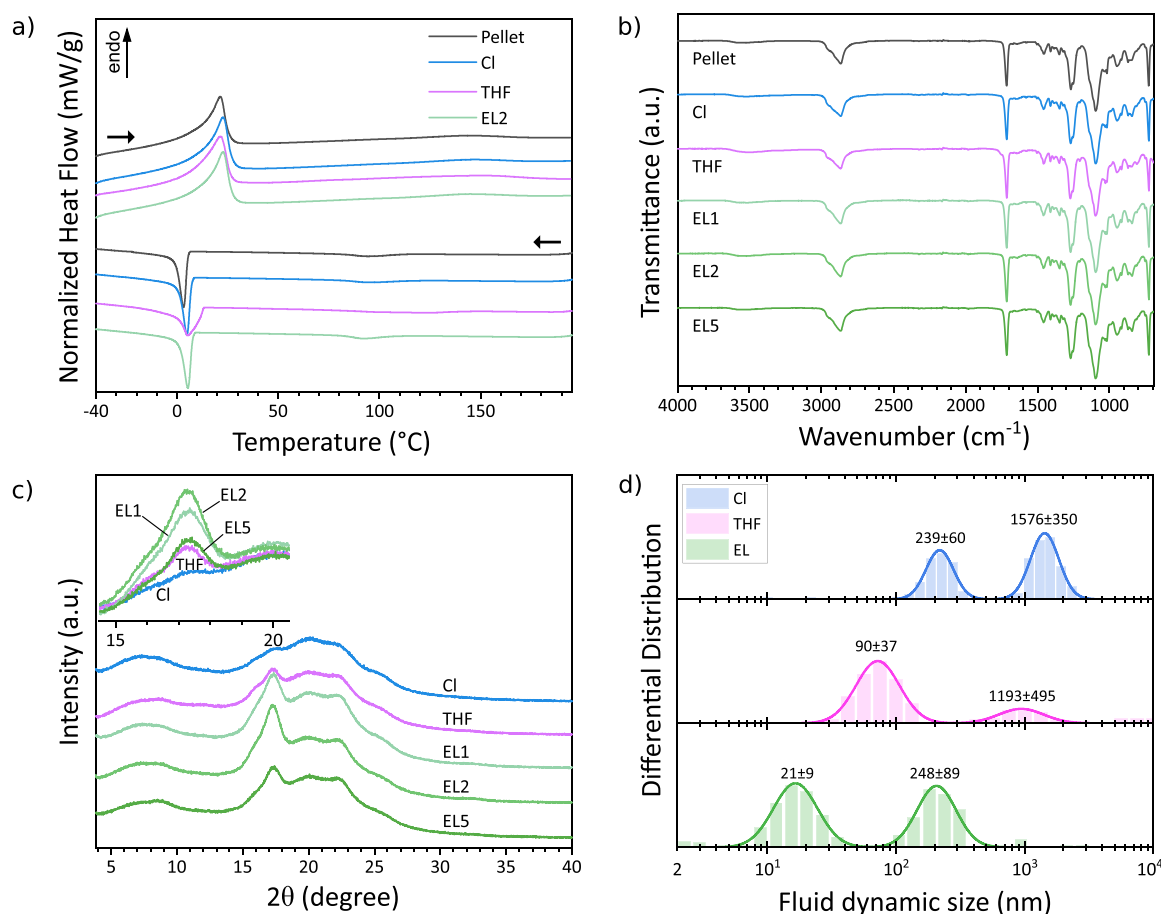


Fig. 2. Characterization of the PolyActive™ pellets and dense membranes. Casting membrane solutions prepared at 2 wt% in chloroform (Cl), tetrahydrofuran (THF) and ethyl lactate at 1, 2 and 5 wt% (EL1, EL2 and EL5, respectively): DSC thermograms for second heating (a, top) and second cooling (a, bottom), ATR-FTIR spectra (b) and XRD patterns with detailed inset at the ca. 17° peak (c). Size distributions obtained by DLS measurements casting solutions where measured at 4 wt% (d).

degree of crystallinity (χ_c) can be estimated as follows with Eq. 11 [54]:

$$\chi_c = \frac{\Delta H_m}{\Delta H_c} \cdot 100 \quad (11)$$

where ΔH_m (in $\text{J} \cdot \text{g}^{-1}$) is the melting enthalpy obtained during the first heating of PEOT blocks, while ΔH_c refers to the theoretical value for a 100 % crystalline PEOT. Although a variety of ΔH_c values can be found in the literature [55,56], the value of $166.4 \text{ J} \cdot \text{g}^{-1}$, as recommended by Simon and Rutherford [57], is widely accepted for this estimation [58,59]. Polymeric chains in a more amorphous state require less energy to melt, resulting in lower measured enthalpies of fusion (ΔH_m) and, consequently, lower crystallinities (χ_c). As shown in Table S1, chloroform and ethyl lactate as solvents led to higher crystallinities in PolyActive™ 1500 membranes (26.4), while the pellet form with THF resulted in lower crystallinity (20.9 and 23.1, respectively). Although the exact conformation for PolyActive™ 1500 pellets is not known, the lower crystallinity is attributed to a faster cooling of the polymer (see below the discussion about the viscosity of polymer solutions as a function of the different solvent used). This allows us to conclude that DSC characterization reveals details, particularly related to polymer-solvent interactions, that TGA analysis alone may overlook.

The FTIR-ATR spectra of the PolyActive™ 1500 membranes and pellets, as depicted in Fig. 2b, reveal the distinct bands corresponding to the PEOT and PBT blocks of the polymer. Due to the similar chemical structures of these segments, some overlapping and broadening of peaks are observed. The polyethylene oxide chain is identified by the intense CH_2 stretching at 2872 cm^{-1} , which also encompasses CH_2 group vibration of PBT as a shoulder peak at 2949 cm^{-1} [60]. Sharp peaks are evident at 1716 cm^{-1} , corresponding to the ester group $\text{C}=\text{O}$ stretching vibration, and at 729 cm^{-1} corresponding possibly to the C-H aromatic ring bending [61]. Additionally, broad stretching peaks with a maximum at 1101 cm^{-1} are associated with CO-C ether bond vibrations, along with the C-O stretching peak at 1269 cm^{-1} [62,63]. The FTIR spectra for the different membranes with various selected solvents show no significant differences.

In Fig. 2c the XRD patterns of the prepared membranes are presented, which show three distinct broad peaks of PEOT-PBT copolymer at 17.3° , 19.9° and 22.3° indicating the existence of crystallinity characteristics in the polymeric membranes, in accordance with literature [26]. When chloroform and THF were used as solvents, they produced the first and second lowest intensities of the initial peak, while ethyl lactate, at the tested concentrations, resulted in higher peak intensities. Notably, the PolyActive™ 1500 membrane at 1 and 2 wt% in ethyl lactate exhibited the highest intensity, as indicated by the most prominent peak. This higher XRD crystallinity when using ethyl lactate is in concordance with the higher DSC crystallinity above mentioned. No changes are observed in the polymer reflections, which indicates that there are no changes in the spacing between polymer chains. These changes in the spacing between polymer chains have been reported when fillers are introduced into the polymer [64].

The viscosity flow curves for the ethyl lactate casting solutions (Figure S3) exhibit a non-Newtonian shear-thinning behavior, characteristic of polymeric solutions. In these curves, the viscosity depends on the shear rate, starting from a zero-shear viscosity (η_0) and decreasing to a plateau at high shear rates (η_∞). The measurements carried out were maintained within the recommended torque range of the viscometer, i. e., between 15 % and 100 %. As a result, the low shear rate region could not be reached, and only the η_∞ values are presented in Table 3. As expected, for all the solvents tested, the casting solutions showed higher viscosities with increasing polymer concentration, and interestingly ethyl lactate had the highest viscosity of the three solvents (23.7 cp), followed by chloroform and THF. A higher viscosity can limit chain mobility during membrane formation, potentially resulting in less ordered crystalline regions within the polymer. However, it also slows solvent evaporation [65], extending the evaporation time and allowing

Table 3

PolyActive viscosity in solution. Viscosities (in cp) at high shear rate (η_∞) for PolyActive™ 1500 casting solutions at different concentrations (0, 1, 2 and 4 wt %) in chloroform, tetrahydrofuran and ethyl lactate measured at 20°C .

Solvent	Concentration (wt%)			
	0	1	2	4
CHCl_3	0.56 ^a	2.23	3.78	14.7
THF	0.46 ^a	- ^a	1.77	2.9
Ethyl lactate	3.00	6.15	9.49	23.7

^a Viscosity values outside the recommended viscometer measurement range. Pure chloroform and tetrahydrofuran values taken from literature.

more time for the polymer chains to self-organize, in line with the DSC findings.

The differential size distributions shown in Fig. 2d were obtained from DLS measurements for PolyActive™ 1500 casting solutions. In sufficiently dilute solutions, linear polymers arrange into isolated coils affected by its solvent compatibility. In good solvents, the polymer swells and occupies more space, while in poor solvents chains curl into a more condensed conformation [66]. DLS measures the apparent size of these open coil conformations, which includes both the polymer and its surrounding solvation shell, referred to as the hydrodynamic (or, more properly speaking, fluid dynamic) diameter [67]. As illustrated in Fig. 2d, the apparent size distribution for PolyActive™ 1500 solutions was the smallest in ethyl lactate, followed by THF and CHCl_3 . Although this might suggest a better dissolution in ethyl lactate, the viscosity of the medium plays a crucial role, potentially leading to inaccurate size estimates. According to the Stoke-Einstein equation, which relates the translation diffusion coefficient measured by DLS to particle size, size is inversely proportional to the viscosity. Typically, solvent viscosity is used for low-concentration DLS measurements, but for high-concentration or non-Newtonian samples, the zero-shear viscosity (η_0) should be considered. Failing to do so may cause the particle size to wrongly seem to depend on solution viscosity [68]. As expected, the DLS analysis revealed polydispersity in all solvents, showing in turn two distinct populations at high and low fluid dynamic radii. Interestingly THF was the least polydisperse (polydispersity index (PDI) of 0.14) compared to ethyl lactate and chloroform, with PDIs of 0.26 and 0.34 respectively. The smaller population is associated with well-dissolved PolyActive™ 1500, while the larger population has been interpreted as undissolved aggregated polymer particles [69,70]. This indicates that THF dissolved the polymer more effectively, in accordance with HSP calculations commented previously, where the Ra value for THF was the lowest of all solvents at a value of $2.3 \text{ MPa}^{0.5}$, followed by CHCl_3 at $3.5 \text{ MPa}^{0.5}$.

AFM air topography measurements (Figure S4) revealed that the cast of membranes using CHCl_3 generated the lowest roughness ($\delta_{\text{RMS}} = 8.7 \text{ nm}$), whereas those prepared with THF and ethyl lactate showed increased roughness values ($\delta_{\text{RMS}} = 11.3 \text{ nm}$ and 11.9 nm , respectively). These results suggest that solvent evaporation dynamics play a crucial role in surface morphology. Specifically, the rapid evaporation of chloroform likely minimizes polymer chain rearrangement and suppresses phase separation, leading to a smoother surface. Conversely, the slower evaporation of THF and ethyl lactate allows for a greater molecular mobility, promoting surface roughness development.

Water contact angle measurements (Figure S4) showed the highest contact angle for ethyl lactate membranes (78.9°), followed by chloroform (63.5°) and THF (56.3°). These values indicate the hydrophilic nature of the polymer, as reported in the literature [71]. The relationship between roughness and contact angle is expected to follow the Wenzel model, where rougher surfaces amplify the intrinsic wettability of the material, making hydrophobic surfaces more hydrophobic and hydrophilic surfaces more hydrophilic. This trend is evident for the THF membranes, which exhibit an increased roughness and a correspondingly slightly lower apparent contact angle (78.7° , 63.3° and 56.0° for

ethyl lactate, chloroform and THF, respectively), consistent with an enhanced hydrophilicity. However, ethyl lactate membranes deviate from this pattern, displaying both higher roughness and a higher contact angle. This suggests that, beyond roughness effects, surface chemistry or polymer crystallinity may also play a significant role. The higher crystallinity observed in ethyl lactate membranes likely results in a more compact, less polar surface, reducing water affinity and leading to a higher contact angle despite the increased roughness.

Fractional free volume (FFV) measurements of the membranes (Table 4) showed that membranes prepared with CHCl_3 and THF exhibited higher FFV values (6.6 % and 6.2 %, respectively), while membranes prepared with ethyl lactate displayed a lower FFV of 4.9 %. For comparison, FFV for PEOT-PBT has been previously estimated using the Positron Annihilation Lifetime Spectroscopy (PALS) technique, showing a value of 3.2 % [36]. It is worth noting that a significant variability in FFV values has been reported for other polymers, such as Pebax® 1657, with an average FFV of 9.6 ± 4.3 % and extremes as high as 16.6 % and as low as 2.6 % [39,72–74]. This variability highlights the sensitivity of FFV measurements to factors such as polymer processing conditions and measurement techniques.

The lower FFV observed for ethyl lactate membranes aligns with the trend of increased crystallinity and a more densely packed polymer structure, as indicated by XRD, DSC and DLS analyses. This supports the hypothesis that the slower evaporation rate achieved with ethyl lactate promotes greater molecular rearrangement and ordering, resulting in a more compact, less porous membrane morphology.

3.3. Single and mixture gas permeation at room temperature

The comparison between the two methods for estimating the gas separation performance of PolyActive™ 1500 membranes is depicted in Fig. 3. This includes single gas permeation using the time-lag method and mixed gas separation assisted by a gas micro-chromatograph for three different gas mixtures of CO_2/N_2 (15:85 vol%, related to post-combustion capture), CO_2/CH_4 (50:50 vol%, linked to biomethane upgrading) and CO_2/H_2 (50:50 vol%, related to pre-combustion capture). As previously mentioned, single gas measurements enable the characterization of membranes in terms of solubility, diffusivity and permeability coefficients. This information is valuable for mathematical modelling and understanding the effect of membrane composition and operating conditions around their apparent solubility and diffusivity. Meanwhile, mixed gas separation provides information into the separation performance with closer practical application, as permeability and separation selectivity can vary when dealing with real post-combustion effluents or biogas-enrichment.

As expected, PolyActive™ 1500 as shown in Fig. 3, and similar to other polyether-block based copolymers, exhibits relatively high CO_2 permeability compared to the other gases [75]. This is due to the strong dipole-quadrupole interaction between the CO_2 molecule and the polyethylene oxide segment, which has greater affinity than N_2 , CH_4 or H_2 . For the post-combustion CO_2/N_2 mixture (at 15:85 vol%), both

Table 4
Densities of PolyActive™ 1500 membranes prepared in different solvents at 2 wt%, obtained by pycnometer measurements. Specific skeletal volume (V_0), specific apparent volume (V) and fractional free volume (FFV) were calculated based on these densities.

Solvent	Skeletal Density ($\text{g}\cdot\text{cm}^{-3}$)	Apparent Density ($\text{g}\cdot\text{cm}^{-3}$)	V_0 ($\text{cm}^3\cdot\text{g}^{-1}$)	V ($\text{cm}^3\cdot\text{g}^{-1}$)	FFV (%)
CHCl_3	1.223	1.142	0.818	0.876	6.6 ± 0.2
THF	1.206	1.132	0.829	0.884	6.2 ± 0.2
Ethyl lactate	1.217	1.158	0.822	0.864	4.9 ± 0.2

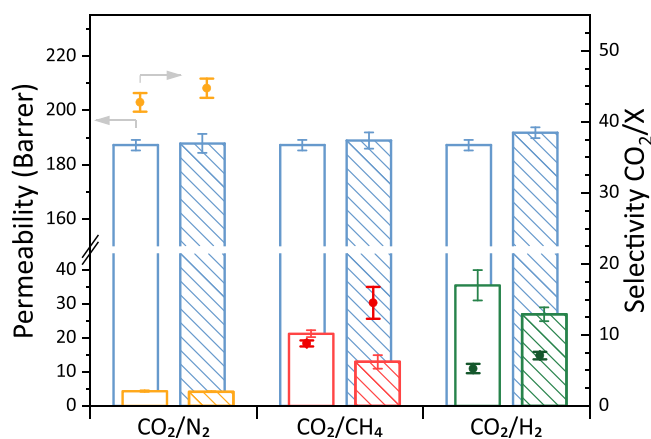


Fig. 3. Gas separation performance of PolyActive™ 1500 chloroform membrane. Measurements of permeability and selectivity for CO_2/N_2 (15:85 vol%), CO_2/CH_4 (50:50 vol%) and CO_2/H_2 (50:50 vol%) mixtures, measured with mixed gases (stripped lines) and single gases (empty) at a feed pressure of 3 bar and a temperature of 35 °C. Membrane casting-solution with CHCl_3 at 2 wt% polymer.

measurements methods indicated a high CO_2 permeability, with single-gas measurements showing 187 ± 3 Barrer and mixed-gas measurements showing 188 ± 4 Barrer. Similarly, for CO_2/CH_4 (50:50 vol %) and CO_2/H_2 (50:50 vol%) mixtures, the CO_2 permeability was approximately 189 ± 3 Barrer and 192 ± 2 Barrer, respectively.

The selectivity of CO_2 in mixture gas separation for all mixtures was higher than that calculated from single gas measurements. As can be seen, while CO_2 permeability is maintained there is a significant decrease in the permeability of the non-selective gases when CO_2 is present in the measurement, improving the separation selectivity. Selectivity for CO_2/N_2 increases from 43 ± 1 to 45 ± 1 , for CO_2/CH_4 from 9 ± 1 to 15 ± 3 and from 5.3 ± 0.7 to 7.1 ± 0.5 for CO_2/H_2 . As shown in Table S2, the separation factors calculated from the permeate concentrations were slightly lower than the separation selectivities derived from mixed gas permeabilities. The measurements were close to ideal conditions, as the stage cut was kept low for all measurements (<0.5 %), which helped minimize concentration polarization on the permeate side. Additionally, the concentration of the more permeable gas (CO_2) remained low, with a maximum of 1.7 vol% in the case of the 50:50 vol% CO_2/H_2 gas separation mixture (Table S2).

The effect of mixed gas selectivity being higher than single gas is mainly caused by a competitive sorption between gaseous species in the polymer matrix [76]. It has been reported in literature [77] that in CO_2/CH_4 separation with poly(1-trimethylsilyl-1-propyne) (PTMSP) polymeric membranes increasing CO_2 partial pressure (fugacity) had a positive and significant effect on the mixed gas solubility selectivity respect to the single gas ideal selectivity. In this direction, the CO_2/N_2 mixture, which has the lowest CO_2 concentration (10 vol%) with respect to the other mixtures CO_2/CH_4 (50 vol%) and CO_2/H_2 (50 vol%), has a lower percentage increase in selectivity. This means that sorption of CO_2 molecules is motivated when higher amounts of it are in the polymeric matrix or more possibly, as the CO_2 permeability remains almost the same, the absorption of the other gas is unfavored because of the presence of the CO_2 molecules. Nevertheless, it has been reported in mixed gas separation at CO_2 fugacities higher than 5 bar that block copolymer blends performed worse due to plasticization effects [78]. It should be noted that here we are working with lower CO_2 pressures (< 3 bar) where the effect of CO_2 swelling is very small. On the contrary, PEG-DA/PEGMEA (another PEG based copolymer) has shown an interesting behavior when exposed from low to high CO_2 partial pressures, maintaining a fixed and equal CO_2/H_2 selectivity during single and mixed gas tests [79]. The effect of better selectivity performances in mixed gas than in single gas based separation has also been reported in literature for other polymeric membranes [80,81] and particularly Pebax® 1657 and

4533 membranes [20], but never before for PolyActive™ membranes.

It is important to note that pure gas measurements involve pressure measurement followed by model fitting using time-lag theory, while mixed gas permeabilities are determined through direct permeation measurements using analytical equipment. Although single-gas measurements may be more straightforward, simple and cost-effective, it is advisable to assess the membrane separation performance under conditions that more closely resemble real-world scenarios (post-combustion, biogas or methanation mixtures) to accurately capture any potential changes in the permeation behavior that might otherwise remain unnoticed.

3.4. Gas separation as a function of temperature

Characterization was conducted by measuring the gas separation performance of the membranes of PolyActive™ 1500 used with a casting solution of CHCl_3 (2 wt%) at various operational temperatures (25, 35, 50 and 70 °C). This temperature range was chosen to ensure the polymer remains within its stable thermal region, preventing changes to either of the copolymer blocks. As shown in the DSC characterization for the PolyActive™ 1500 membranes (Fig. 2a), the PEOT block exhibits a pronounced melting peak at room temperature. For PEOT-PBT copolymers, CO_2 permeance increases above the melting transition of the polyethylene oxide block, enhancing both permeability and selectivity for CO_2/N_2 separations [59]. Additionally, a hysteresis effect occurs, where the polymer maintains a higher permselectivity within this temperature range even slightly below the melting temperature of PEOT [53]. To revert to the initial state, it is necessary to cool the material to the crystallization temperature, which is 10–15 °C lower.

When the polymeric membranes do not undergo phase transition the relationship between permeability and temperature follows Eq. 5 with an Arrhenius tendency. Therefore, in Fig. 4 the permeabilities of gases were plotted against the inverse of the temperature and adjusted to a

linear regression so the corresponding apparent activation energies of permeation from the slope could be obtained (Eq. 12):

$$\ln P_i = \ln P_{0,i} - \frac{E_{P,i}}{R} \cdot \frac{1}{T} \quad (12)$$

Apparent activation energies of permeation for all gases have been collected in Table 5. As can be seen from these values, higher values of E_P (like that of CH_4) translate into a higher slope in the temperature dependence of permeability shown in Fig. 4. This means that, due to carbon dioxide having a lower activation energy than the other gases, ideal selectivity drops for CO_2/X mixtures when increasing temperature, having the highest gas ideal selectivity at the lowest tested temperature of 25 °C (Fig. 4, top).

An equivalent procedure can be followed for diffusivity obtained through the time-lag method and the linearization of Eqs. 6 and 7 where apparent activation energy of diffusion (E_D) and enthalpy of sorption (ΔH_S) can be calculated with the following Eqs. 13 and 14:

$$\ln D_i = \ln D_{0,i} - \frac{E_{D,i}}{R} \cdot \frac{1}{T} \quad (13)$$

$$\ln S_i = \ln S_{0,i} - \frac{\Delta H_{S,i}}{R} \cdot \frac{1}{T} \quad (14)$$

In Fig. 5, temperature dependences for the diffusion (top) and solubility (bottom) coefficients are presented, along with their respective linear regressions. Note that the solubility coefficients were derived from Eq. 4 and are not direct measurements obtained via the time-lag technique; they were calculated using the permeability and diffusion coefficients. The determination of diffusion coefficients for highly diffusive species such as H_2 and He was challenging due to the small time-lag values (calculated from the intersection of the extrapolated steady-state pressure curve with the horizontal axis), resulting in higher errors in their determination. This also led to an unexpected temperature dependence for the solubility coefficients, where these species exhibited an apparent slight increase in solubility with rising temperature. However, the CO_2 molecule, which has been mentioned is solubilized in the polymer, shows an abrupt decrease in solubility with temperature. This solubility is also a fundamental parameter for the separation of CO_2 from other gases with lower solubilities.

Table 5 summarizes the permeability, diffusion, and solubility coefficients at the lowest tested temperature, along with the activation energies calculated using the linear fitting of the Arrhenius equation. The diffusion coefficients indicate that smaller molecules, such as H_2 and He , diffuse less obstructed through the matrix, while larger molecules like CO_2 , N_2 , and CH_4 , with greater kinetic diameters, exhibit lower apparent diffusion coefficients. Also, as shown in Figure S5, the activation energies of diffusion increase proportionally with the effective cross-section of the gas molecules, what is consistent with previous literature [82]. This trend indicates that smaller molecules have lower activation energies compared to larger ones. This behavior can be attributed to the free volume created by the PEOT chains within the polymer matrix. All single gas measurements of permeability, diffusion, and solubility at various temperatures are presented in Table S3 of the Supporting Information (SI).

As expected, the solubility coefficient of CO_2 , $21.1 \cdot 10^{-3} \text{ cm}^3 \cdot (\text{STP}) \cdot \text{cm}^{-3} \cdot \text{cmHg}^{-1}$, is at least around 10 times greater than those of the other gases. It can be inferred that the primary mechanism enabling the high ideal selectivity of the PolyActive™ membrane for CO_2 in CO_2/N_2 , CO_2/CH_4 and CO_2/H_2 separations is not the difference in diffusivity, as the values are relatively similar. Rather, it is the strong affinity of the soft block of the copolymer with CO_2 that enhances CO_2 solubility, facilitating the selective transport. This is confirmed by examining the diffusion and solubility selectivities presented in Table 6. The diffusion selectivity $\alpha(D)$ for CO_2 is around 0.9 when separating it from N_2 and CH_4 , while it is approximately 0.5 for H_2 separation, showing minimal dependence with the temperature. In contrast, solubility selectivities

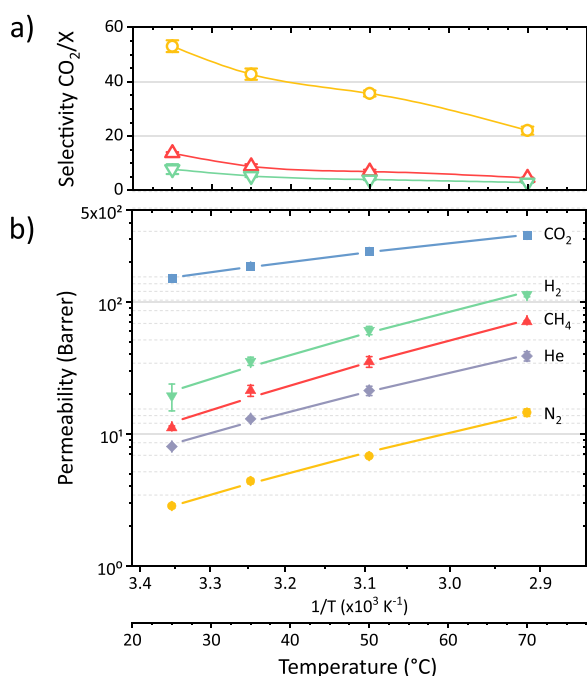


Fig. 4. Ideal selectivity and permeability dependence with temperature of pure gases for PolyActive™ 1500 membranes. Ideal selectivity (a) is calculated for CO_2/N_2 (yellow), CO_2/CH_4 (red) and CO_2/H_2 (green) mixtures from single gas measurements, solid line serves as visual aid. Permeability (b) shows CO_2 (blue), H_2 (green), CH_4 (red), He (grey) and N_2 (yellow) with their respective linear regressions in following a temperature activated process (Eq. 12). Membrane casting-solution with CHCl_3 at 2 wt% polymer.

Table 5

Gas transport properties and activation energies for PolyActive™ 1500. Permeability P, diffusion D and solubility S of gases measured at 25 °C and activation energies of permeabilities E_P , diffusion E_D and enthalpy of sorption ΔH_S for PolyActive™ 1500 calculated with Eqs. 12, 13 and 14.

Gas	P (Barrer)	E_P (kJ·mol ⁻¹)	D (10 ⁻⁶ ·cm ² ·s ⁻¹)	E_D (kJ·mol ⁻¹)	S (10 ⁻³ ·cm ³ (STP)·cm ⁻³ ·cmHg ⁻¹)	ΔH_S (kJ·mol ⁻¹)
He	8.0	29.4	2.03	21.4	0.39	10.6
H ₂	19.4	32.7	1.56	23.2	1.25	6.9
CO ₂	151	14.2	0.72	25.9	21.1	-12.1
N ₂	2.8	30.3	0.71	26.9	0.39	-5.1
CH ₄	11.1	33.9	0.70	31.8	2.20	-3.0

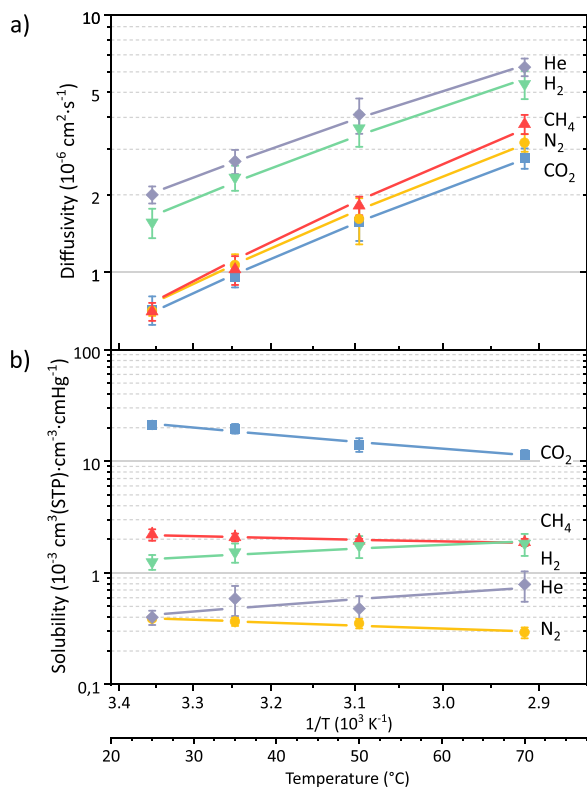


Fig. 5. Effective diffusivity and solubility dependence with temperature of pure gases for PolyActive™ 1500 membranes. Diffusivity (a) and solubility (b) values for CO₂ (blue), CH₄ (red), H₂ (green), He (grey) and N₂ (yellow) are shown with their respective linear regressions following Eqs. 13 and 14, respectively.

$\alpha(S)$ are significantly higher (up to 56) and influenced by increasing temperature, as indicated by the increased activation energy values, $E(\alpha)$. The low $\alpha(D)$ values among the gas species indicate potential avenues for improving or modifying the membrane material to enhance its performance. By developing materials that selectively hinder the diffusion of certain molecules within the membrane and given the already high $\alpha(S)$ of CO₂, $\alpha(D)$ can be further improved. This approach has been

demonstrated by Sabetghadam et al. [64] with Cu-BDC nanosheets used as filler in PolyActive™ MMMs for CO₂/N₂ separation.

3.5. Solvent effect in gas permeation properties

Single gas permeation measurements were conducted on PolyActive™ 1500 membranes prepared using different solvents (CHCl₃, THF and ethyl lactate) at 35 °C and a 3 bar feed pressure. Fig. 6 presents the measured permeabilities obtained via the time-lag method, along with the ideal selectivities calculated for CO₂. Membranes dissolved in CHCl₃ and THF demonstrated similar CO₂ permeability at approximately 187 Barrer, with comparable CO₂/N₂ ideal selectivity 39–42. In contrast, ethyl lactate at 1, 2 and 5 wt% polymer concentrations resulted in a significant reduction in CO₂ and N₂ permeability of the membranes, but with an overall increase in ideal selectivity up to 50.6 for 1 and 2 wt %, and 46.9 for 5 wt%. Despite the reduced permeability for ethyl lactate membranes, the improvement in ideal selectivity was primarily observed for CO₂ mixtures with the less permeable gases, N₂ and He. Additionally, THF membranes showed higher permeability for gases other than CO₂, leading to a slight decrease in ideal selectivity for CO₂/

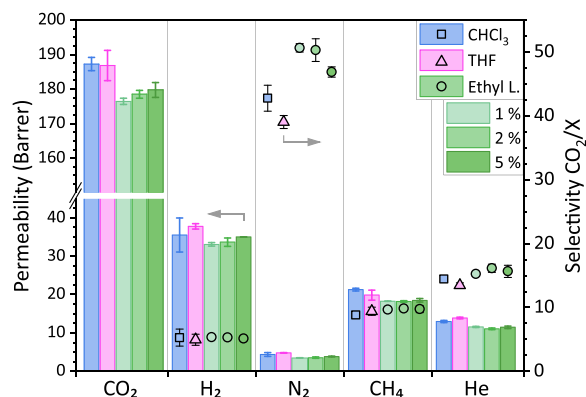


Fig. 6. Solvent effect on permeability and ideal selectivity in gas separation. Gas permeability of CO₂, H₂, N₂, CH₄ and He (bars) and ideal selectivity of CO₂/X mixtures (symbols) tested at 35 °C with single gas measurements of PolyActive™ 1500 membranes using different solvents: chloroform (2 wt%, blue), THF (2 wt%, pink) and ethyl lactate (1, 2 and 5 wt%, green).

Table 6

Gas transport selectivity coefficients dependance with temperature. Permeability, diffusion and solubility ideal selectivities calculated from pure gas at the temperatures tested and corresponding activation energy selectivities for PolyActive™ 1500 membranes using chloroform as solvent. The equations for these calculations can be found in Table S4.

Gas	CO ₂ /N ₂			—	CO ₂ /CH ₄			—	CO ₂ /H ₂		
	$\alpha(P)$	$\alpha(D)$	$\alpha(S)$		$\alpha(P)$	$\alpha(D)$	$\alpha(S)$		$\alpha(P)$	$\alpha(D)$	$\alpha(S)$
T (°C)											
25	53.1	1.01	54.6		13.6	1.02	9.61		7.77	0.46	16.89
35	42.8	0.78	53.5		8.8	0.93	9.43		5.27	0.41	12.81
50	35.7	0.97	40.0		6.9	0.86	7.30		3.98	0.43	8.09
70	22.0	0.87	39.6		4.5	0.74	6.16		2.81	0.52	6.33
$E(\alpha)$ (kJ mol ⁻¹)	-16	-1.0	-7.0		-20	-5.9	-9.1		-19	2.7	-19.0

H₂ and CO₂/He mixtures. However, for the CO₂/CH₄ separation, the methane permeability was lower, and the THF membrane demonstrated an ideal selectivity of 9.4 comparable to that of the ethyl lactate membrane (9.8). As discussed in the membrane characterization section, CHCl₃ and THF dissolved the polymer more effectively, as indicated by HSP calculations and DLS measurements. This resulted in membranes with reduced crystallinity, as confirmed by XRD and DSC analyses. The lower crystallinity increases the fractional free volume, further supported by the pycnometry measurements. The greater free volume between polymer chains facilitates the diffusion of smaller gas molecules, leading to higher permeability and a corresponding decrease in ideal selectivity in N₂, H₂ and He separations.

Examining the effect of polymer concentration on permeability for ethyl lactate membranes revealed an increase in the permeability of most gases, though still lower than that for membranes with CHCl₃ and THF (Table S5 provides detailed permeabilities). This increase in permeation correlates with a decrease in CO₂/N₂ ideal selectivity as polymer concentration rises. As no solvent residue was detected in membrane characterization, this behavior may be attributed to variations in the polymer crystallinity influenced by the selected solvent and its concentration. According to the literature [83], crystalline polymers are generally less permeable than amorphous ones, often exhibiting higher selectivities. Different solvents used in creating polymeric films can affect the packing of the polymeric chains, significantly impacting the membrane separation performance due to their properties such as molecular weight, molar volume, and boiling point. Specifically, as seen in viscosity measurements of ethyl lactate casting solutions at 20 °C, lower polymer concentrations in the casting solution (same mass of polymer is dissolved with more quantity of solvent) could increase evaporation times and reduce viscosity, allowing the polymeric chains to form more crystalline and packed structures. Conversely, higher polymer concentrations reduce the solvent evaporation time, and the increased solution viscosity hinders polymeric chain mobility, creating more free space and facilitating an easier molecular movement through the matrix. The higher evaporation rates, due to lower viscosities and boiling points, of CHCl₃ and THF compared to ethyl lactate also explain their higher permeabilities and reduced ideal selectivity similarly.

Apparent diffusion and solubility coefficients are presented as a function of casting solution concentration in CHCl₃, THF and ethyl lactate in Fig. 7. The solubility of CO₂ in all three solvents was similar at around $19.5 \cdot 10^{-3} \text{ cm}^3(\text{STP}) \cdot \text{cm}^{-3} \cdot \text{cmHg}^{-1}$. However, a decrease in diffusivity is observed for ethyl lactate membranes, which accounts for the aforementioned drop in permeability. As polymer concentration

increases, diffusivity also increased, with the same trend evident for the other gases. As stated, lower polymer concentrations during the evaporation process in membrane casting allow for chains to order themselves in a more compacted crystalline material. Notably, gases with high diffusivities, such as He and H₂, led to less accurate measurements with significant data point dispersion at 2 wt%. In contrast, the solubility remained relatively unaffected by polymer concentration, staying constant. The higher ideal selectivities observed for the CO₂/N₂ separation can be mainly attributed to the lower solubility of N₂ in the ethyl lactate membranes compared to CHCl₃ and THF membranes. The smaller FFV of ethyl lactate, as seen previously, hinders the gas transport as commented, but particularly for less soluble gases like N₂, as they are less compatible with the polymer; in consequence, the swelling of the polymer and permeation through it becomes more difficult.

Notably, values for CO₂ gas transport parameters for PolyActive™ 1500 dense membranes obtained using the time-lag method by different authors are compared in Table 7 with the values of the membrane prepared with the green solvent ethyl lactate. CO₂ permeabilities show similar behavior for ethyl lactate prepared in this work (179 Barrer) and THF prepared in [10] (181 Barrer), suggesting that both solvents have a comparable membrane performance. In contrast, membranes fabricated in the literature with chloroform exhibit a lower CO₂ permeability (115–169 Barrer), generally lower than those corresponding to ethyl lactate and THF previously commented. Interestingly, the lowest permeability (115 Barrer) corresponds to the lowest pressure condition (0.3 bar), reflecting a possible pressure dependence of permeability. Despite this, chloroform membranes maintain a relatively high ideal selectivity (45.6–57.1), with the highest values aligning with lower temperature conditions (25 and 30 °C), so that our ideal selectivity was achieved at a higher temperature (35 °C), justifying the relatively lower value of 50.4.

CO₂ solubility remains consistently high across all samples, reflecting the strong affinity for CO₂ of PolyActive™ 1500. Values range between 17.5 and $22.2 \times 10^{-3} \text{ cm}^3(\text{STP}) \cdot \text{cm}^{-3} \cdot \text{cmHg}^{-1}$, with ethyl lactate (20.1) performing on par with THF (19.9) and surpassing generally the lower chloroform solubilities in the literature (17.5 and 18.5). This suggests that while chloroform maintains a good ideal selectivity, it may compromise the CO₂ uptake slightly. CO₂ diffusivity shows more variation, spanning from 0.62 to $0.91 \times 10^{-6} \text{ cm}^2 \cdot \text{s}^{-1}$, where ethyl lactate (0.89) and THF (0.91) exhibit again a comparable performance, while chloroform samples in the literature present lower diffusivities (0.62–0.90), aligning with their lower permeability values.

Interestingly, chloroform-based membranes display close ideal

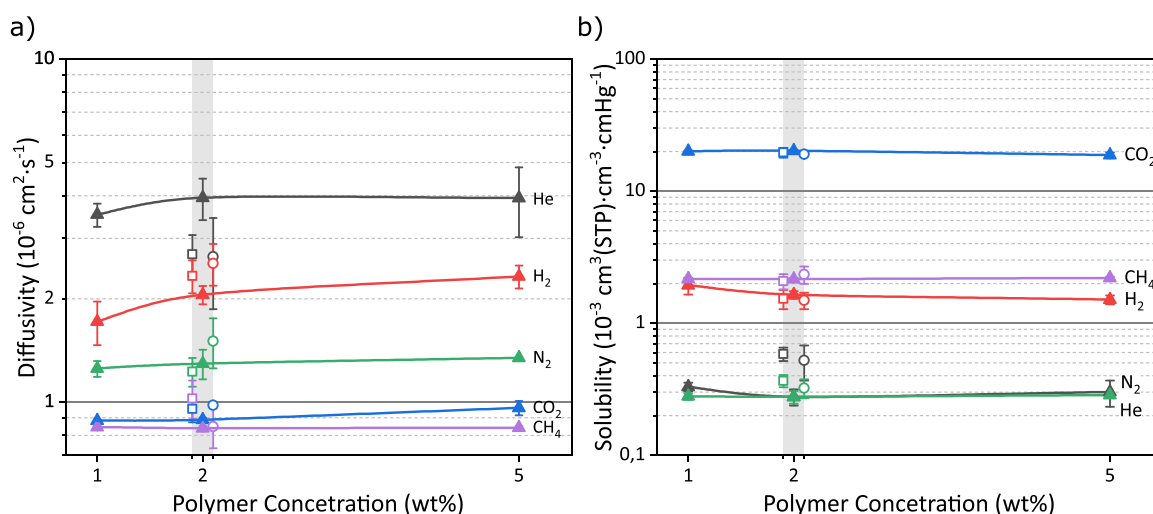


Fig. 7. Polymer concentration and solvent dependence of diffusivity (left) and solubility (right). Values for CO₂ (blue), H₂ (red), N₂ (green), CH₄ (purple) and He (grey) measured at 35 °C and 3 bar pressure feed for PolyActive™ 1500 membranes using different solvents: chloroform (□), THF (○) and ethyl lactate (▲). Error bars for solubility were calculated from error propagation.

Table 7

Comparison of gas separation performance for PolyActive™ 1500 membranes from literature. CO₂ permeability (P_{CO₂}), diffusivity (D_{CO₂}), solubility (S_{CO₂}) and CO₂/N₂ ideal selectivity (α_{CO₂/N₂}) are shown for 1500PEOT23-PBT77 membranes, with all data obtained from single gas time-lag measurements. Solvents used for membrane preparation and testing conditions, including temperature (T) and pressure (P), are also presented.

Solvent	Permeation parameters		Transport parameters		Testing conditions		Ref.
	P _{CO₂} (Barrer)	α _{CO₂/N₂}	D _{CO₂} (10 ⁻⁶ .cm ² .s ⁻¹)	S _{CO₂} (10 ⁻³ .cm ³ (STP).cm ⁻³ .cmHg ⁻¹)	T (°C)	P (bar)	
Ethyl lactate	179	50.4	0.89	20.1	35	3	This study
THF	181	53.2	0.91	19.9	30	0.8	[10]
CHCl ₃	160	57.1	0.90	17.5	25	1	[75]
CHCl ₃	169	56.3	0.75	22.2	30	1	[59]
CHCl ₃	115	45.6	0.62	18.5	30	0.3	[9]

selectivity values (57.1 and 56.3) despite being tested at different temperatures (25 °C and 30 °C). Given the strong temperature dependence of ideal selectivity discussed earlier, this consistency is unexpected, as a more pronounced variation would typically be observed. The lower-pressure chloroform dataset (0.3 bar) further expands this observation, showing a reduced CO₂ permeability (115 Barrer) alongside with a drop in ideal selectivity (45.6). Differences in temperature, pressure and fabrication conditions, together with potential deviations in membrane morphology or measurement setups, underscore the importance of cautious interpretation when benchmarking the membrane performance across several studies.

4. Conclusions

Among the selection of solvents tested, ethyl lactate has been found as an alternative green solvent for PolyActive™ 1500 (1500PEOT77-PBT23) from other commonly used solvents such as CHCl₃ and THF. The casting-solution method for membrane fabrication with ethyl lactate required the dissolution of the polymer pellets under reflux for 4 h at 80 °C. TGA measurements confirmed that the thermal degradation was identical for pristine pellets and dense membranes prepared in CHCl₃ and THF, showing no degradation below 200 °C. Also, the DSC analysis confirmed the thermal stability and semicrystalline state of the polymer in the working temperature range for gas separation, where PEOT soft and PBT hard blocks are above and below their fusion temperatures, respectively. Importantly, the physicochemical characterization carried out showed that the ethyl lactate membranes were more crystalline than the ones prepared with other solvents, corroborated by higher intensity peaks in XRD and DSC crystallinity estimations of the polymeric membranes. Also, the DLS size particle analysis on polymer casting solutions showed that THF dissolved the polymer more effectively (aggregated population showed lowest distribution intensity), while ethyl lactate gave rise to lower particle sizes indicating less swelling of the polymer chains and a poorer polymer dissolution. Membranes prepared with chloroform are the least hydrophilic and the roughest, showing a lower free volume, which is related to their greater crystallinity.

Gas transport parameters (permeability, diffusion and solubility) of PolyActive™ 1500 in chloroform, measured using the time-lag method over a temperature range of 25–70 °C, followed an activated temperature process. As anticipated, CO₂ exhibited the highest permeability due to its high compatibility with the polymer, showing a solubility 10 times greater than that of the other gases. The apparent activation energy for gas diffusion was found to depend on the square of the effective gas diameter. In mixed gas measurements using binary mixtures, the CO₂ permeability remained similar to the value achieved in single gas tests, though higher selectivities were observed and were attributed to the competitive adsorption of CO₂ with the less permeable species. Membranes prepared using ethyl lactate resulted in higher ideal selectivities but lower permeabilities, with CO₂ permeability decreasing from 187 to 176 Barrer. This behavior is related to the increased crystallinity and lower FFV of the ethyl lactate membranes, which reduced the gas

diffusivity, particularly at lower polymer concentrations in the casting solutions (1 and 2 wt%). Increased crystallinity is attributed to a closer packing of polymer chains obtained by longer evaporation times due to the higher boiling point of ethyl lactate.

This work demonstrates that ethyl lactate can be a greener alternative to traditional solvents for fabrication of PolyActive™ 1500 membranes, offering the potential for more environmentally friendly and less toxic processes. Its use could provide advantages in membrane formation, particularly for thin-film composite membranes, without compromising the membrane performance.

CRedit authorship contribution statement

Téllez Carlos: Writing – review & editing, Writing – original draft, Supervision, Resources, Project administration, Methodology, Funding acquisition, Conceptualization. **Martínez-Visus Íñigo:** Writing – review & editing, Writing – original draft, Visualization, Validation, Methodology, Investigation, Formal analysis. **Coronas Joaquín:** Writing – review & editing, Writing – original draft, Supervision, Resources, Project administration, Methodology, Funding acquisition, Conceptualization.

Declaration of Competing Interest

The authors declare that they have no known competing financial interests or personal relationships that could have appeared to influence the work reported in this paper.

Acknowledgement

This work gratefully acknowledges grants PID2022-138582OB-I00 (funded by MICIU/AEI/10.13039/501100011033/ and by “ERDF A way of making Europe”), PID2019-104009RB-I00 (funded by MICIU/AEI/10.13039/501100011033) and CEX2023-001286-S (funded by MICIU/AEI/10.13039/501100011033/). I. Martínez-Visus was supported through grant PRE2020-092006 (funded by MCIN/AEI/10.13039/501100011033 and by “ESF Investing in your future”). Financial assistance from the Government of Aragón (T68_23R) is also acknowledged. Authors would like to acknowledge the use of Servicio General de Apoyo a la Investigación-SAI, Universidad de Zaragoza, and the use of instrumentation as well as the technical advice provided by the National Facility ELECMI ICTS, node «Laboratorio de Microscopías Avanzadas (LMA)» at «Universidad de Zaragoza». Finally, Prof. Dr Steven Abbott is thanked for providing estimation of Hansen solubility parameters of PolyActive™.

Appendix A. Supporting information

Supplementary data associated with this article can be found in the online version at [doi:10.1016/j.jece.2025.116893](https://doi.org/10.1016/j.jece.2025.116893).

Data availability

Data will be made available on request.

References

- [1] L. Nunes, The rising threat of atmospheric CO₂: a review on the causes, impacts, and mitigation strategies, *Environments* 10 (2023) 66, <https://doi.org/10.3390/environments10040066>.
- [2] G.A. Meehl, T.F. Stocker, W.D. Collins, P. Friedlingstein, A.T. Gaye, J.M. Gregory, A. Kitoh, R. Knutti, J.M. Murphy, A. Noda, S.C.B. Raper, I.G. Watterson, A. J. Weaver, Z.C. Zhao, Global Climate Projections, in: S. Solomon, D. Qin, M. Manning, Z. Chen, M. Marquis, K.B. Averyt, M. Tignor, H.L. Miller (Eds.), *Climate Change 2007: The Physical Science Basis. Contribution of Working Group I to the Fourth Assessment Report of the Intergovernmental Panel on Climate Change*, Cambridge University Press, Cambridge, United Kingdom and New York, NY, USA, 2007.
- [3] R. Maniarasu, S.K. Rathore, S. Murugan, A review on materials and processes for carbon dioxide separation and capture, *Energy Environ. Sci.* 14 (1) (2021) 3–57, <https://doi.org/10.1039/C1EE01000A>.
- [4] C. Chao, Y. Deng, R. Dewil, J. Baeyens, X. Fan, Post-combustion carbon capture, *Renew. Sustain. Energy Rev.* 138 (2021) 110490, <https://doi.org/10.1016/j.rser.2020.110490>.
- [5] A. Naquash, M.A. Qyyum, Y.D. Chaniago, A. Riaz, F. Yehia, H. Lim, M. Lee, Separation and purification of syngas-derived hydrogen: a comparative evaluation of membrane- and cryogenic-assisted approaches, *Chemosphere* 313 (2023) 137420 <https://doi.org/10.1016/j.chemosphere.2022.137420>.
- [6] O. Purrucker, J. Balster, Hydrogen on Tap: Supporting Decarbonization by Pipelining H₂ to the Point of Use, Q4 Report, Linde Engineering, Pullach, Germany, 2021.
- [7] P. Gkotsis, E. Peleka, A. Zouboulis, Membrane-based technologies for post-combustion CO₂ capture from flue gases: recent progress in commonly employed membrane materials, *Membranes* 13 (2023) 898, <https://doi.org/10.3390/membranes13120898>.
- [8] M.G. Buonomenna, W. Yave, G. Golemme, Some approaches for high performance polymer based membranes for gas separation: block copolymers, carbon molecular sieves and mixed matrix membranes, *RSC Adv.* 2 (29) (2012) 10745–10773, <https://doi.org/10.1039/C2RA20748F>.
- [9] A. Car, C. Stropnik, W. Yave, K.-V. Peinemann, Tailor-made polymeric membranes based on segmented block copolymers for CO₂ separation, *Adv. Funct. Mater.* 18 (18) (2008) 2815–2823, <https://doi.org/10.1002/adfm.200800436>.
- [10] J. Liljeblom, P. Georgopoulos, S. Shishatskiy, Stability of blended polymeric materials for CO₂ separation, *J. Membr. Sci.* 467 (2014) 269–278, <https://doi.org/10.1016/j.memsci.2014.05.039>.
- [11] T. Brinkmann, J. Liljeblom, H. Notzke, J. Pohlmann, S. Shishatskiy, J. Wind, T. Wolff, Development of CO₂ selective poly(ethylene oxide)-based membranes: from laboratory to pilot plant scale, *Engineering* 3 (4) (2017) 485–493, <https://doi.org/10.1016/j.eng.2017.04.004>.
- [12] F. Brennecke, J. Clodt, T. Brinkmann, V. Abetz, Numerical and experimental investigation of the unexpected thickening effect during PolyActive™ coating of TFC membranes, *J. Adv. Manuf. Process.* 6 (2) (2024) e10175, <https://doi.org/10.1002/amp2.10175>.
- [13] X. He, D. Chen, Z. Liang, F. Yang, Insight and comparison of energy-efficient membrane processes for CO₂ capture from flue gases in power plant and energy-intensive industry, *Carbon Capture Sci. Technol.* 2 (2022) 100020, <https://doi.org/10.1016/j.cst.2021.100020>.
- [14] T. Peters, L. Ansaloni, M. Rosa De La Viuda, A. Tena, O. Karvan, T. Visser, D. Chinn, N. Bhuvanana, Performance and stability of selected polymeric membrane materials for use in high-H₂S and humid natural gas feeds, *Ind. Eng. Chem. Res.* 64 (6) (2025) 3441–3452, <https://doi.org/10.1021/acs.iecr.4c03485>.
- [15] H.A. Daynes, The process of diffusion through a rubber membrane, *Proc. R. Soc. Lond. Ser. A Contain. Pap. A Math. Phys. Character* 97 (685) (1920) 286–307, <https://doi.org/10.1098/rspa.1920.0034>.
- [16] M. Khan, S. Shishatskiy, V. Filiz, Mixed matrix membranes of boron icosahedron and polymers of intrinsic microporosity (PIM-1) for gas separation, *Membranes* 8 (1) (2018), <https://doi.org/10.3390/membranes8010001>.
- [17] J. Sanchez, C.L. Gijji, V. Hynek, O. Muntean, A. Julbe, The application of transient time-lag method for the diffusion coefficient estimation on zeolite composite membranes, *Sep. Purif. Technol.* 25 (1) (2001) 467–474, [https://doi.org/10.1016/S1383-5866\(01\)00076-4](https://doi.org/10.1016/S1383-5866(01)00076-4).
- [18] C. Damian, E. Espuche, M. Escoubes, Influence of three ageing types (thermal oxidation, radiochemical and hydrolytic ageing) on the structure and gas transport properties of epoxy-amine networks, *Polym. Degrad. Stab.* 72 (3) (2001) 447–458, [https://doi.org/10.1016/S0141-3910\(01\)00045-3](https://doi.org/10.1016/S0141-3910(01)00045-3).
- [19] A. Akbari, J. Karimi-Sabet, S.M. Ghoreishi, Matrimid® 5218 based mixed matrix membranes containing metal organic frameworks (MOFs) for helium separation, *Chem. Eng. Process. Process. Intensif.* 148 (2020) 107804, <https://doi.org/10.1016/j.ccep.2020.107804>.
- [20] L. Martínez-Izquierdo, A. Perea-Cachero, M. Malankowska, C. Téllez, J. Coronas, A comparative study between single gas and mixed gas permeation of polyether-block-amide type copolymer membranes, *J. Environ. Chem. Eng.* 10 (5) (2022) 108324, <https://doi.org/10.1016/j.jece.2022.108324>.
- [21] S.A. Naziri Mehrabani, V. Vatanpour, I. Koyuncu, Green solvents in polymeric membrane fabrication: a review, *Sep. Purif. Technol.* 298 (2022) 121691, <https://doi.org/10.1016/j.seppur.2022.121691>.
- [22] W. Yave, A. Szymczyk, N. Yave, Z. Roslaniec, Design, synthesis, characterization and optimization of PTT-b-PEO copolymers: a new membrane material for CO₂ separation, *J. Membr. Sci.* 362 (1) (2010) 407–416, <https://doi.org/10.1016/j.memsci.2010.06.060>.
- [23] D.M. Nedeljković, M.P. Stevanović, M.Z. Stijepović, A.P. Stajčić, A.S. Grujić, J. T. Stajčić-Trošić, J.S. Stevanović, The possibility of the application of the zeolite powders for the construction of the membranes for the carbon dioxide separation, *Chem. Ind. Chem. Eng. Q.* 21 (2) (2015) 277–284, <https://doi.org/10.2298/CICEQ130924025N>.
- [24] W. Yave, A. Car, S.S. Funari, S.P. Nunes, K.-V. Peinemann, CO₂-philic polymer membrane with extremely high separation performance, *Macromolecules* 43 (1) (2010) 326–333, <https://doi.org/10.1021/ma901950u>.
- [25] M. Karunakaran, R. Shevate, M. Kumar, K.V. Peinemann, CO₂-selective PEO-PBT (PolyActive™)/graphene oxide composite membranes, *Chem. Commun.* 51 (75) (2015) 14187–14190, <https://doi.org/10.1039/C5CC04999G>.
- [26] M. Shan, B. Seane, E. Andres-Garcia, F. Kapteijn, J. Gascon, Mixed-matrix membranes containing an azine-linked covalent organic framework: Influence of the polymeric matrix on post-combustion CO₂-capture, *J. Membr. Sci.* 549 (2018) 377–384, <https://doi.org/10.1016/j.memsci.2017.12.008>.
- [27] M. Liu, K. Xie, M.D. Nothling, P.A. Gurr, S.S.L. Tan, Q. Fu, P.A. Webley, G.G. Qiao, Ultrathin metal-organic framework nanosheets as a gutter layer for flexible composite gas separation membranes, *ACS Nano* 12 (11) (2018) 11591–11599, <https://doi.org/10.1021/acsnano.8b06811>.
- [28] W. Yave, A. Car, J. Wind, K.-V. Peinemann, Nanometric thin film membranes manufactured on square meter scale: ultra-thin films for CO₂ capture, *Nanotechnology* 21 (39) (2010) 395301, <https://doi.org/10.1088/0957-4484/21/39/395301>.
- [29] P.T. Anastas, J.C. Warner, Oxford England. *Green chemistry: theory and practice*, Oxford University Press, 1998.
- [30] E. Lasseguette, J.-C. Rouch, J.-C. Remigy, Hollow-fiber coating: application to preparation of composite hollow-fiber membrane for gas separation, *Ind. Eng. Chem. Res.* 52 (36) (2013) 13146–13158, <https://doi.org/10.1021/ie401874m>.
- [31] U.T. Syed, L. Upadhyaya, L.M.D. Loiola, A.-H. Emwas, A. Volkov, S.P. Nunes, Thymol: nature's solvent for sustainable hollow fiber fabrication, *Green. Chem.* 26 (23) (2024) 11576–11586, <https://doi.org/10.1039/D4GC01961J>.
- [32] P.V. Chai, Y.K. Ku, W.J. Chan, Preparation of enhanced antifouling graphene oxide cellulose acetate mixed-matrix membrane using ethyl lactate green solvent, *AIP Conf. Proc.* 2945 050001 (1) (2023), <https://doi.org/10.1063/5.0185435>.
- [33] J. Saleem, Z.K.B. Moghal, R. Luque, G. McKay, Towards green membranes: repurposing waste polypropylene with a single plant-based solvent via tandem spin-casting and annealing, *Chem. Eng. J.* 481 (2024) 148560, <https://doi.org/10.1016/j.ccej.2024.148560>.
- [34] G. Gomez d'Ayala, T. Marino, Y.M. de Almeida, A.R. Costa, L. Bezerra da Silva, P. Argurio, P. Laurienzo, Enhancing sustainability in PLA membrane preparation through the use of biobased solvents, *Polymers* 16 (14) (2024), <https://doi.org/10.3390/polym16142024>.
- [35] F. Galiano, A.H. Ghanim, K.T. Rashid, T. Marino, S. Simone, Q.F. Alsalhi, A. Figoli, Preparation and characterization of green polylactic acid (PLA) membranes for organic/organic separation by pervaporation, *Clean. Technol. Environ. Policy* 21 (1) (2019) 109–120, <https://doi.org/10.1007/s10098-018-1621-4>.
- [36] W. Yong, Y. un Ho, T. i-Shung Chung, Nanoparticles embedded in amphiphilic membranes for carbon dioxide separation and dehumidification, *ChemSusChem* 10 (20) (2017) 4046–4055, <https://doi.org/10.1002/cssc.201701405>.
- [37] P. Cools, M. Asadian, W. Nicolaus, H. Declercq, R. Morent, N. De Geyter, Surface treatment of PEOT/PBT (55/45) with a dielectric barrier discharge in air, helium, argon and nitrogen at medium pressure, *Materials* 11 (3) (2018) 391, <https://doi.org/10.3390/ma11030391>.
- [38] L.C.H. Moh, J.B. Goods, Y. Kim, T.M. Swager, Free volume enhanced proton exchange membranes from sulfonated triptycene poly(ether ketone), *J. Membr. Sci.* 549 (2018) 236–243, <https://doi.org/10.1016/j.memsci.2017.11.041>.
- [39] L. Dong, M. Chen, J. Li, D. Shi, W. Dong, X. Li, Y. Bai, Metal-organic framework-graphene oxide composites: a facile method to highly improve the CO₂ separation performance of mixed matrix membranes, *J. Membr. Sci.* 520 (2016) 801–811, <https://doi.org/10.1016/j.memsci.2016.08.043>.
- [40] R.M. Barrer, *Diffusion in and through solids*, The University Press, 1941.
- [41] S.V. Dixon-Garrett, K. Nagai, B.D. Freeman, Sorption, diffusion, and permeation of ethylbenzene in poly(1-trimethylsilyl-1-propyne), *J. Polym. Sci. Part B Polym. Phys.* 38 (8) (2000) 1078–1089, [https://doi.org/10.1002/\(SICI\)1099-0488\(20000415\)38:8<1078::AID-POLB8>3.0.CO;2-2](https://doi.org/10.1002/(SICI)1099-0488(20000415)38:8<1078::AID-POLB8>3.0.CO;2-2).
- [42] R.M. Barrer, E.K. Rideal, Permeation, diffusion and solution of gases in organic polymers, *Trans. Faraday Soc.* 35 (1939) 628–643, <https://doi.org/10.1039/tf9393500628>.
- [43] S.A. Stern, W.P. Walawender, Analysis of membrane separation parameters, *Sep. Sci.* 4 (2) (1969) 129–159, <https://doi.org/10.1080/01496396908052244>.
- [44] V. Stannett, The transport of gases in synthetic polymeric membranes — an historic perspective, *J. Membr. Sci.* 3 (2) (1978) 97–115, [https://doi.org/10.1016/S0376-7388\(00\)83016-1](https://doi.org/10.1016/S0376-7388(00)83016-1).
- [45] J. Liljeblom, E. Sperling, M. Blanke, M. Held, S. Shishatskiy, J. Liljeblom, E. Sperling, M. Blanke, M. Held, S. Shishatskiy, Multicomponent network formation in selective layer of composite membrane for CO₂ separation, *Membranes* 11 (2021) 174, <https://doi.org/10.3390/membranes11030174>.

- [46] C.S.M. Pereira, V.M.T.M. Silva, A.E. Rodrigues, Ethyl lactate as a solvent: properties, applications and production processes – a review, *Green. Chem.* 13 (10) (2011) 2658–2671, <https://doi.org/10.1039/C1GC15523G>.
- [47] L.J. Diorazio, D.R.J. Hose, N.K. Adlington, Toward a more holistic framework for solvent selection, *Org. Process Res. Dev.* 20 (4) (2016) 760–773, <https://doi.org/10.1021/acs.oprd.6b00015>.
- [48] Y. Alqaheem, A. Alomair, A. Alhend, S. Alkandari, N. Tanoli, N. Alnajdi, A. Quesada-Pérez, Preparation of polyetherimide membrane from non-toxic solvents for the separation of hydrogen from methane, *Chem. Cent. J.* 12 (1) (2018) 80, <https://doi.org/10.1186/s13065-018-0449-7>.
- [49] B.D. Freeman, I. Pinnau, Polymeric Materials for Gas Separations, in: *Polymer Membranes for Gas and Vapor Separation*, American Chemical Society, 1999, pp. 1–27, <https://doi.org/10.1021/bk-1999-0733.ch001>.
- [50] A. Tena, S. Shishatskiy, V. Filiz, Poly(ether–amide) vs. poly(ether–imide) copolymers for post-combustion membrane separation processes, *RSC Adv.* 5 (29) (2015) 22310–22318, <https://doi.org/10.1039/c5ra01328c>.
- [51] M. Klepić, A. Fuoco, M. Monteleone, E. Esposito, K. Friess, Z. Petrusová, P. Izák, J. C. Jansen, Tailoring the thermal and mechanical properties of PolyActive™ poly(ether–ester) multiblock copolymers via blending with CO₂-philic ionic liquid, *Polymers* 12 (4) (2020) 890, <https://doi.org/10.3390/polym12040890>.
- [52] S. Fakirov, T. Gogeva, Poly(ether/ester)s based on poly(butylene terephthalate) and poly(ethylene glycol), 1. Poly(ether/ester)s with various polyether: polyester ratios, *Die Makromol. Chem.* 191 (3) (1990) 603–614, <https://doi.org/10.1002/macp.1990.021910315>.
- [53] M.M. Rahman, C. Abetz, S. Shishatskiy, J. Martin, A.J. Müller, V. Abetz, CO₂ selective PolyActive membrane: thermal transitions and gas permeance as a function of thickness, *ACS Appl. Mater. Interfaces* 10 (31) (2018) 26733–26744, <https://doi.org/10.1021/acsami.8b09259>.
- [54] Y. Kong, J.N. Hay, The measurement of the crystallinity of polymers by DSC, *Polymer* 43 (14) (2002) 3873–3878, [https://doi.org/10.1016/S0032-3861\(02\)00235-5](https://doi.org/10.1016/S0032-3861(02)00235-5).
- [55] B. Wunderlich, *Thermal Analysis*, Elsevier Science, 2012.
- [56] J. Brandrup, E.H. Immergut, E.A. Grulke, *Polymer Handbook*, 4th ed., Wiley, New York, 1999.
- [57] F.T. Simon, J.M. Rutherford, Crystallization and melting behavior of polyethylene oxide copolymers, *J. Appl. Phys.* 35 (1) (1964) 82–86, <https://doi.org/10.1063/1.1713103>.
- [58] H. Lin, B.D. Freeman, Gas solubility, diffusivity and permeability in poly(ethylene oxide), *J. Membr. Sci.* 239 (1) (2004) 105–117, <https://doi.org/10.1016/j.memsci.2003.08.031>.
- [59] M.M. Rahman, V. Filiz, S. Shishatskiy, C. Abetz, P. Georgopoulos, M.M. Khan, S. Neumann, V. Abetz, Influence of poly(ethylene glycol) segment length on CO₂ permeation and stability of PolyActive membranes and their nanocomposites with PEG POSS, *ACS Appl. Mater. Interfaces* 7 (23) (2015) 12289–12298, <https://doi.org/10.1021/am504223f>.
- [60] S. Zivanovic, J. Li, P.M. Davidson, K. Kit, Physical, mechanical, and antibacterial properties of chitosan/PEO blend films, *Biomacromolecules* 8 (5) (2007) 1505–1510, <https://doi.org/10.1021/bm061140p>.
- [61] I. Irska, S. Paszkiewicz, K. Goracy, A. Linares, T. Ezquerro, R. Jedrzejewski, Z. Roslaniec, E. Piesowicz, Poly(butylene terephthalate)/polylactic acid based copolymers and blends: miscibility-structure-property relationship, *EXPRESS Polym. Lett.* 14 (2020) 26–47, <https://doi.org/10.3144/expresspolymlett.2020.4>.
- [62] Y.-K. Fuh, S. Chen, J.S.C. Jang, Direct-write, well-aligned chitosan-poly(ethylene oxide) nanofibers deposited via near-field electrospinning, *J. Macromol. Sci., Part A* 49 (10) (2012) 845–850, <https://doi.org/10.1080/10601325.2012.714676>.
- [63] H. Sanaeepur, S. Mashhadikhan, G. Mardassi, A. Ebadi Amooghin, B. Van der Bruggen, A. Moghadassi, Aminosilane cross-linked poly ether-block-amide PEBAX 2533: characterization and CO₂ separation properties, *Korean J. Chem. Eng.* 36 (8) (2019) 1339–1349, <https://doi.org/10.1007/s11814-019-0323-x>.
- [64] A. Sabetghadam, X. Liu, S. Gottmer, L. Chu, J. Gascon, F. Kapteijn, Thin mixed matrix and dual layer membranes containing metal-organic framework nanosheets and Polyactive™ for CO₂ capture, *J. Membr. Sci.* 570 (571) (2019) 226–235, <https://doi.org/10.1016/j.memsci.2018.10.047>.
- [65] Y. Zhang, Z. Zhang, J. Yang, Y. Yue, H. Zhang, Evaporation characteristics of viscous droplets on stainless steel superhydrophobic surface, *Int. J. Therm. Sci.* 183 (2023) 107843, <https://doi.org/10.1016/j.jthermalsci.2022.107843>.
- [66] F. Monroy, L.R. Arriaga, D. Langevin, Langmuir polymer films: recent results and new perspectives, *Phys. Chem. Chem. Phys.* 14 (42) (2012) 14450–14459, <https://doi.org/10.1039/C2CP42454A>.
- [67] Malvern Panalytical, Polymer Characterization Using Light Scattering Techniques. AZoNano. (<https://www.azonano.com/article.aspx?ArticleID=1232>). (Accessed March 25, 2025).
- [68] I. Buriša Instruments, Viscosity Effects in Dynamic Light Scattering Measurements, Technical Note, Horiba Instruments, Inc., Irvine, CA, USA, 2004.
- [69] B. Swensson, S. Lages, B. Berke, A. Larsson, M. Hasani, Scattering studies of the size and structure of cellulose dissolved in aqueous hydroxide base solvents, *Carbohydr. Polym.* 274 (2021) 118634, <https://doi.org/10.1016/j.carbpol.2021.118634>.
- [70] S. Chakraborty, B. Sahoo, I. Teraoka, R.A. Gross, Solution properties of starch nanoparticles in water and DMSO as studied by dynamic light scattering, *Carbohydr. Polym.* 60 (4) (2005) 475–481, <https://doi.org/10.1016/j.carbpol.2005.03.011>.
- [71] I. Buitinga, R. Truckenmüller, M.A. Engelse, L. Moroni, H.W.M. Ten Hoopen, C. A. van Blitterswijk, E.J.P. de Koning, A.A. van Apeldoorn, M. Karperien, Microwell Scaffolds for the extrahepatic transplantation of islets of langerhans, *PLOS ONE* 8 (5) (2013) e64772, <https://doi.org/10.1371/journal.pone.0064772>.
- [72] S. Meshkat, S. Kaliaguine, D. Rodrigue, Mixed matrix membranes based on amine and non-amine MIL-53(Al) in Pebax® MH-1657 for CO₂ separation, *Sep. Purif. Technol.* 200 (2018) 177–190, <https://doi.org/10.1016/j.seppur.2018.02.038>.
- [73] R.S. Murali, S. Sridhar, T. Sankarshana, Y.V.L. Ravikumar, Gas permeation behavior of pebax-1657 nanocomposite membrane incorporated with multiwalled carbon nanotubes, *Ind. Eng. Chem. Res.* 49 (14) (2010) 6530–6538, <https://doi.org/10.1021/ie9016495>.
- [74] A. Tayebi, A. Kargari, S. Akbari, Enhancing the performance of a modified poly(ether-b-amide) blend membrane by PAMAM dendritic polymer for separation of CO₂/CH₄, *Polym. Test.* 128 (2023) 108225, <https://doi.org/10.1016/j.polymertesting.2023.108225>.
- [75] M. Klepić, A. Fuoco, M. Monteleone, E. Esposito, K. Friess, P. Izák, J.C. Jansen, Effect of the CO₂-philic ionic liquid [BMIM][Tf₂N] on the single and mixed gas transport in PolyActive™ membranes, *Sep. Purif. Technol.* 256 (2021) 117813, <https://doi.org/10.1016/j.seppur.2020.117813>.
- [76] C. Rizzuto, A. Caravella, A. Brunetti, C.H. Park, Y.M. Lee, E. Drioli, G. Barbieri, E. Tocci, Sorption and Diffusion of CO₂/N₂ in gas mixture in thermally-rearranged polymeric membranes: a molecular investigation, *J. Membr. Sci.* 528 (2017) 135–146, <https://doi.org/10.1016/j.memsci.2017.01.025>.
- [77] O. Vopicka, M.G. De Angelis, G.C. Sarti, Mixed gas sorption in glassy polymeric membranes: 1. CO₂/CH₄ and n-C₄/CH₄ mixtures sorption in poly(1-trimethylsilyl-1-propyne) (PTMSP), *J. Membr. Sci.* 449 (2014) 97–108, <https://doi.org/10.1016/j.memsci.2013.06.065>.
- [78] S.R. Reijerkerk, M.H. Knoef, K. Nijmeijer, M. Wessling, Poly(ethylene glycol) and poly(dimethyl siloxane): combining their advantages into efficient CO₂ gas separation membranes, *J. Membr. Sci.* 352 (1) (2010) 126–135, <https://doi.org/10.1016/j.memsci.2010.02.008>.
- [79] H. Lin, E. Van Wagner, B.D. Freeman, L.G. Toy, R.P. Gupta, Plasticization-enhanced hydrogen purification using polymeric membranes, *Science* 311 (5761) (2006) 639–642, <https://doi.org/10.1126/science.1118079>.
- [80] S. Thomas, I. Pinnau, N. Du, M.D. Guiver, Hydrocarbon/hydrogen mixed-gas permeation properties of PIM-1, an amorphous microporous spirobisindane polymer, *J. Membr. Sci.* 338 (1) (2009) 1–4, <https://doi.org/10.1016/j.memsci.2009.04.021>.
- [81] R. Swaidan, X. Ma, E. Litwiller, I. Pinnau, High pressure pure- and mixed-gas separation of CO₂/CH₄ by thermally-rearranged and carbon molecular sieve membranes derived from a polyimide of intrinsic microporosity, *J. Membr. Sci.* 447 (2013) 387–394, <https://doi.org/10.1016/j.memsci.2013.07.057>.
- [82] V. Teplyakov, P. Meares, Correlation aspects of the selective gas permeabilities of polymeric materials and membranes, *Gas. Sep. Purif.* 4 (2) (1990) 66–74, [https://doi.org/10.1016/0950-4214\(90\)80030-O](https://doi.org/10.1016/0950-4214(90)80030-O).
- [83] M. Isanejad, N. Azizi, T. Mohammadi, Pebax membrane for CO₂/CH₄ separation: effects of various solvents on morphology and performance, *J. Appl. Polym. Sci.* 134 (9) (2017), <https://doi.org/10.1002/app.44531>.